Since January 2020 Elsevier has created a COVID-19 resource centre with free information in English and Mandarin on the novel coronavirus COVID-19. The COVID-19 resource centre is hosted on Elsevier Connect, the company's public news and information website.

Biomaterials 287 (2022) 121666

Contents lists available at ScienceDirect

Biomaterials

journal homepage: www.elsevier.com/locate/biomaterials

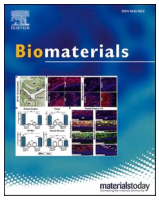

Fibrous aggregates: Amplifying aggregation-induced emission to boost health protection

Zhenduo Qiu [1], Xiaoxiao Yu [1], Junyan Zhang, Chengjian Xu, Mengyue Gao, Yanhua Cheng [*], Meifang Zhu

State Key Laboratory for Modification of Chemical Fibers and Polymer Materials, College of Materials Science and Engineering, Donghua University. Shanghai, 201620, China

ARTICLE INFO

Keywords:
Fibers
Aggregation-induced emission
Sensing
Therapy
Health protection

ABSTRACT

Environmental monitoring and personal protection are critical for preventing and for protecting human health during all infectious disease outbreaks (including COVID-19). Fluorescent probes combining sensing, imaging and therapy functions, could not only afford direct visualizing existence of biotargets and monitoring their dynamic information, but also provide therapeutic functions for killing various bacteria or viruses. Luminogens with aggregation-induced emission (AIE) could be well suited for above requirements because of their typical photophysical properties and therapeutic functions. Integration of these molecules with fibers or textiles is of great interest for developing flexible devices and wearable systems. In this review, we mainly focus on how fibers and AIEgens to be combined for health protection based on the latest advances in biosensing and bioprotection. We first discuss the construction of fibrous sensors for visualization of biomolecules. Next recent advances in therapeutic fabrics for individual protection are introduced. Finally, the current challenges and future opportunities for "AIE + Fiber" in sensing and therapeutic applications are presented.

1. Introduction

According to the guidance for the infection prevention and control by World Health Organization: "safe water, sanitation and waste management and hygienic conditions is essential for preventing and for protecting human health during all infectious disease outbreaks, including of coronavirus disease 2019 (COVID-19)" [1]. Therefore, environmental monitoring and personal protection are necessary. Fluorescent probes combining functions of sensing, imaging and therapy, could not only afford direct visualizing the existence of biotargets and monitoring their dynamic information [2–5], but also provide therapeutic functions for killing various bacteria or viruses [6,7]. In this regard, many designs and synthetic approaches have been developed for functional fluorescent probes, for example, quantum dots [8], metal-containing complexes [9], and organic fluorophores [10]. Among them, organic fluorophores show advantages because of good biocompatibility and flexible molecular modification [11]. However, for most traditional organic dyes, their emission or therapeutic function are normally quenched or reduced in aggregate state. This phenomenon is known as aggregation-induced quenching (ACQ) [12], which seriously limits their performance in biological application, leading to unsatisfactory outcomes.

In contrast to traditional ACQ fluorophores, aggregation-induced emission luminogens (AIEgens) are weakly or non-emissive when they are isolated in good solvent, but "lit-up" when they aggregate (Fig. 1a) [13]. Restriction of intramolecular motion (RIM) is considered as working mechanism for AIEgens, which impresses the nonradiative energy dissipation to promote fluorescence [14]. This unique feature makes them potential to be applied for biological sensing and imaging [15,16]. In addition, through rational chemical design, AIEgens could be further endowed with photosensitization effect and photothermal capability (Fig. 1b) [17,18]. Traditional AIEgen could be immediately designed as photosensitizers (PSs) with introduction of donor-acceptor (D-A) structure, leading to the reduced energy gap (ΔE_{ST}) between triplet and singlet excited state (S_1-T_1), activating the intersystem crossing (ISC) process accordingly [19]. AIE PSs could both improve fluorescence and reactive oxygen species (ROS) production at aggregate state, revealing unique advantages during practical applications.

* Corresponding author.
E-mail address: cyh@dhu.edu.cn (Y. Cheng).
[1] Zhenduo Qiu and Xiaoxiao Yu contributed equally to this work.

https://doi.org/10.1016/j.biomaterials.2022.121666
Received 3 May 2022; Received in revised form 25 June 2022; Accepted 29 June 2022
Available online 4 July 2022

Besides, owing to the rotor structures, AIEgens also could be transformed into photothermal agents (PTAs) by activating intramolecular motions [20]. By introduction of D-A structure, planar skeleton, and alkyl chains into AIEgens, the light-harvesting ability and nonradiative decay could be further activated, resulting in excellent photothermal conversion efficiency [21,22].

In the past decades, advanced synthetic strategies at the molecular level have been extensively used to develop multifunctional AIEgens [23,24]. Integration of these molecules with fibers or textiles is of great interest for developing flexible devices and wearable systems (Fig. 1c). Fibers, especially synthetic polymer fibers, characterized with high aspect ratio and high surface area [25,26], is a kind of long and thin thread of material that could be knit or woven into a fabric [27,28]. The fluorescent probes are directly embedded into or grafted onto fibers, showing high interface to interact with analytes and thereby exhibiting high sensitivity and fast responsibility, which may have a synergistic effect with polymer matrix [29,30]. Fibrous-based fluorescent sensors are easy-readable, sensitive and flexible to conveniently integrate into portable devices [31], benefitting for family and individual self-testing. Moreover, additional functional enzyme catalysts could be separately decorated on the surface of fibers to develop Janus fibers or double layer fabrics, consequently further boosting the sensing performance [32,33].

On the other hand, fibers could be engineered to modify their chemical composition and physical structure during the manufacturing process, which providing suitable microenvironment to manipulate the intramolecular motion of AIEgens and then promoting the nonradiative decays to boost ROS production and photothermal efficiency. In the recent design, core-shell structure fibers and three-dimensional nanofibrous aerogels were recently developed, which further improve photothermal conversion efficiency of the dopped PTAs because of the enhanced nonradiative decay process [34,35]. The developed fibrous membranes mediated by photodynamic and photothermal therapy show great potential in wound dressings, self-sterilizing protection, and hot patches.

In this review, we focus on the recent advances in the synergy of "AIE + Fiber" for health protection from aspect of AIE probes selection and fiber structure engineering. Firstly, we discuss the construction of AIE fibrous sensors for visualization of small molecules, proteins, and bacteria. Then we introduce recent representative examples of therapeutic fabrics for individual protection. Finally, we give our perspectives regarding the challenges and future opportunities for "AIE + Fiber" in potential sensing and therapeutic applications.

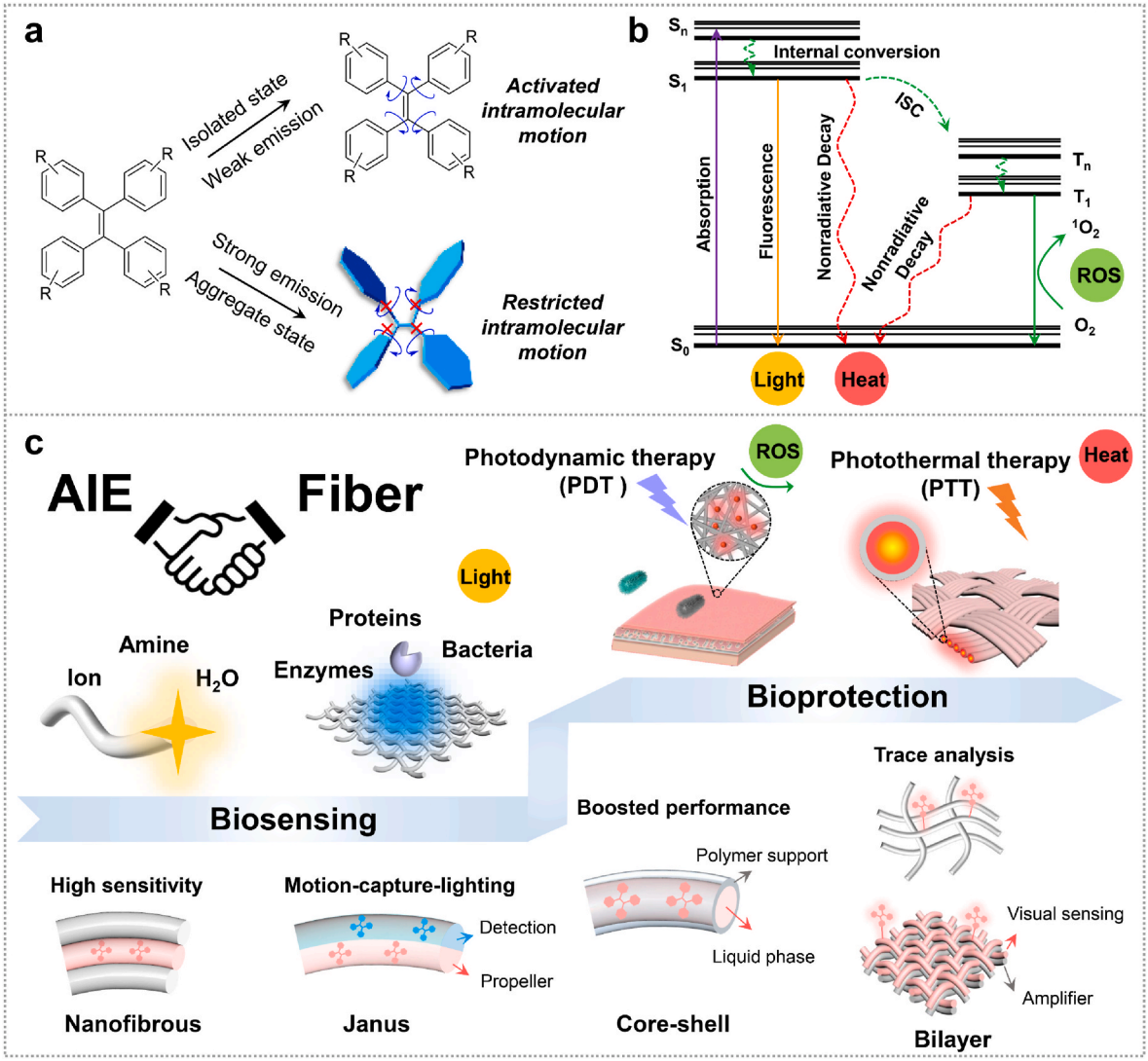

Fig. 1. Illustration of AIE working mechanism and applications of the "AIE + Fiber". (a) Restriction of intramolecular motions of AIEgens for "light-up" in aggregate state. (b) Simplified Jablonski diagram of the electronic transition of AIEgens (radiative decay), AIE PSs (ISC process) and AIE PTAs (nonradiative decay). (c) An overview of "AIE + Fiber" for health protection in terms of biosensing and bioprotection.

2. Sensing

Fluorescent biomolecular sensing and detection play vital roles in indicating biological state and evaluating living environment, providing a sensitive, accurate, and easy-readable way for trace amounts of analytes sensing. Many fluorescence detection methods have been reported by using small molecules individually [36,37]. However, most of the existing molecular probes have been dispersed in biological fluids for working, which are not suitable for visual and portable detection. Fibers (especially electrospun nanofibers), characterized by high surface-area-to-volume ratios, are attractive candidates to combine with AIEgens for constructing sensors with high sensitivities, rapid responses, and great simplicity [38,39]. AIE probes are integrated with fibers for sensing in two forms, one is directly doping into fibers, another is grafting onto the surface of fibers. For the first one, the analytes are mostly in gas form, which could penetrate into the polymer matrix of fibers to interact with AIE probes [30], generating visible signals to be detected. For the latter one, the analytes are usually dispersed in aqueous phase [40]. The grafted AIE probes are normally designed with a hydrophilic group (*e.g.*, phosphate, sulfonate, quaternary ammonium), ensuring the good dispersibility for fully contact with analytes. In addition, these probes could also be decorated with targeting or reactive groups to improve the specificity to targets. Meanwhile, the fibrous substrates provide an anchor to stabilize AIE probes, benefiting for on-site, portable, and individual self-testing. These resulted "AIE + Fiber" sensors have high potential to be integrated into the wearable system. In this section, the sensing targets or analytes could be roughly divided into three groups: i) small molecules such as biogenic amines, sugars, ions and water vapor; ii) functional macromolecules such as proteins and enzymes; iii) bioorganisms such as *E. coli* bacteria (Fig. 1c).

Small molecules. Biogenic amines have gained recognition not only as indirect indicators of food freshness but also to be linked with episodes of food intoxication [43]. These biogenic amines with low molecular weight including one or more amine groups, are produced by microbial, vegetable and animal metabolisms [44,45]. To detect these compounds, most of the existing fluorescent probes have been designed to work in liquid state [46]. However, these approaches are not suitable for portable detection. Incorporating the fluorescent probes into membrane or film represents good solution to be assembled with devices, which showing high surface area to fully contact with the gas for highly sensitive detection. Tang et al. reported an amine-specific pen-like portable sensor with a fiber detector in the device (Fig. 2a), which was developed by decoration of amine responsive AIEgens (DQ_2) on the fiber detector by a sol-gel process [41]. Sol-gel coatings on the silicon dioxide (SiO_2) fiber provide a rigid scaffold for immobilization of fluorescent probes of DQ_2 (Fig. 2b). The immobilized DQ_2 was first to react with trifluoroacetic acid (TFA) to produce protonated form of H^+DQ_2 and quench the emission accordingly. After exposure to amine vapor, nitrogen deprotonation was occurred and the yellow emission was turned on (Fig. 2c). This system was demonstrated to withdrawn inside for protection and pushed out for detection, and successfully used for solid-state amine portable detection from salmon fish. The sensitivity was determined to be 0.2 ppm. However, because of the dense structure of the organosilica coating, the penetration of analytes vapor was

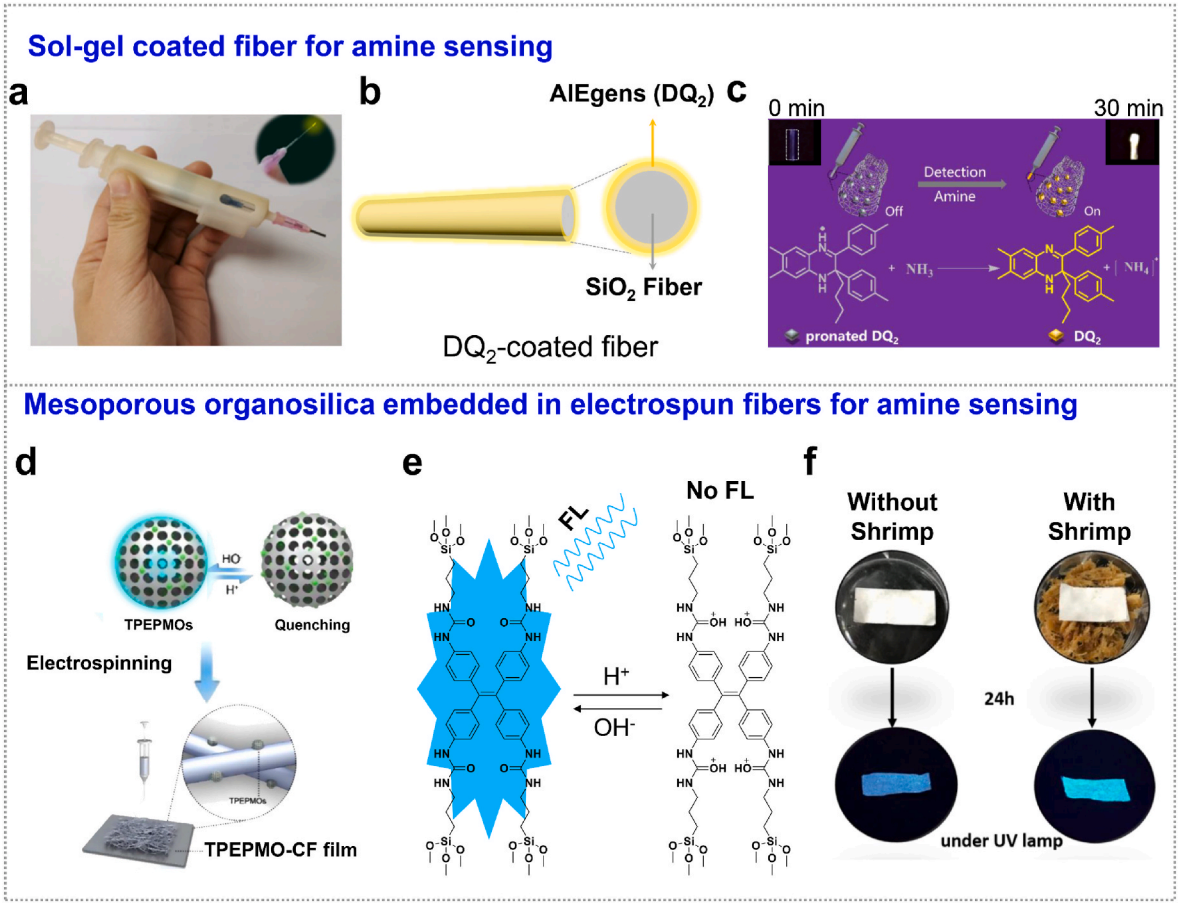

Fig. 2. Biogenic amine detection. (a) AIE handy pen for visual detection of amine vapor. (b) DQ_2-immobilized sol-gel coatings on the SiO_2 fiber. (c) Mechanism for amine detection by sol-gel coatings. Insets: Fibers exposed to 20 ppm amine for 0 and 30 min under UV lamp. Adapted and reproduced with permission from Ref. [41]. Copyright 2021 American Chemical Society. (d) Mesoporous AIEgen-organosilica embedded electrospun nanofibers for amine sensing; (e) Mechanism for amine detection by reversible protonation of AIE probes. (f) Nanofibrous sensor for shrimp spoilage monitoring. Adapted and reproduced with permission from Ref. [42]. Copyright 2021 American Chemical Society.

blocked at some extent, resulting in the slow response time (5 min for amine detection).

Kong et al. used periodic mesoporous organosilica (PMO) to assemble with pH-sensitive fluorescent molecules (TPEPMOs) for amine sensing (Fig. 2d), owing to abundant reaction sites provided by highly porous PMO for rapid and sensitive detection [42]. The resulted TPEPMO nanoparticles were then embedded into the PLGA (poly (lactic-*co*-glycolic acid)) or PAN (polyacrylonitrile) for subsequent electrospinning. The fluorescence quenching of the TPE unit was caused by reversible protonation of TPEPMOs (Fig. 2e), with a linear correlation between fluorescence intensity and pH in the range of 3.9–4.7. Upon exposing the fibrous membrane sensors to ammonia vapor, the fluorescence recovered and the detection limit was estimated to be 15 mg/m^3. This "turn-on" process for amine detection was reversible, and was demonstrated to monitor food spoilage processes (*e.g.*, shrimp freshness) for health protection (Fig. 2f). In addition, the nanofibrous network endowed the sensors wearability, stability, and washability (fluorescence maintained above 94% after 10 times washing), but at the expense of response time because the polymer network of nanofibers blocked the mass transfer in TPEPMO nanoparticles.

Metal ions are important in biological process [47–49]. The contamination of heavy metal ions such as mercury ions (Hg^{2+}) is a serious problem because they are extremely toxic even at low concentrations [50,51]. Therefore, simple, fast and selective monitoring of trace Hg^{2+} is highly needed for environmental safety and health diagnosis [52]. Compared with the Hg^{2+} detection by using small molecules that dispersed in aqueous solution, grafting fluorescent probes on test papers show advantages to construct self-test devices for an on-site, visual, and portable detection. Nanofibrous strip is a potential candidate as the immobilizer to promote the sensitivity and response time because of the large surface area and high network porosity [53]. Taking these advantages of fibrous substrate, Li et al. developed TPE derivatives containing sulfonic groups and carboxyl dithioacetals to introduce on the surface of polystyrene-*co*-maleic anhydride (PSMA) and polystyrene (PS) blended electrospun fibers [40] (Fig. 3a). The AIE activities of the grafted TPE derivatives were initiated to show bright emission, which was attributed by the short spacer chains between AIE probes and fiber surface to restrict the intramolecular motions of TPE units. Owing to the strong thiophilic affinity with Hg^{2+}, the dithioacetal moieties were gradually cleaved and then TPE derivatives (containing sulfonate groups) were released from fibers. The water-soluble residues significantly decreased emission intensities accordingly. Such "turn-off" emission fibrous sensor could be fitted into an equation versus Hg^{2+} concentrations, enabling a visual and quantitative sensing (Fig. 3b). The

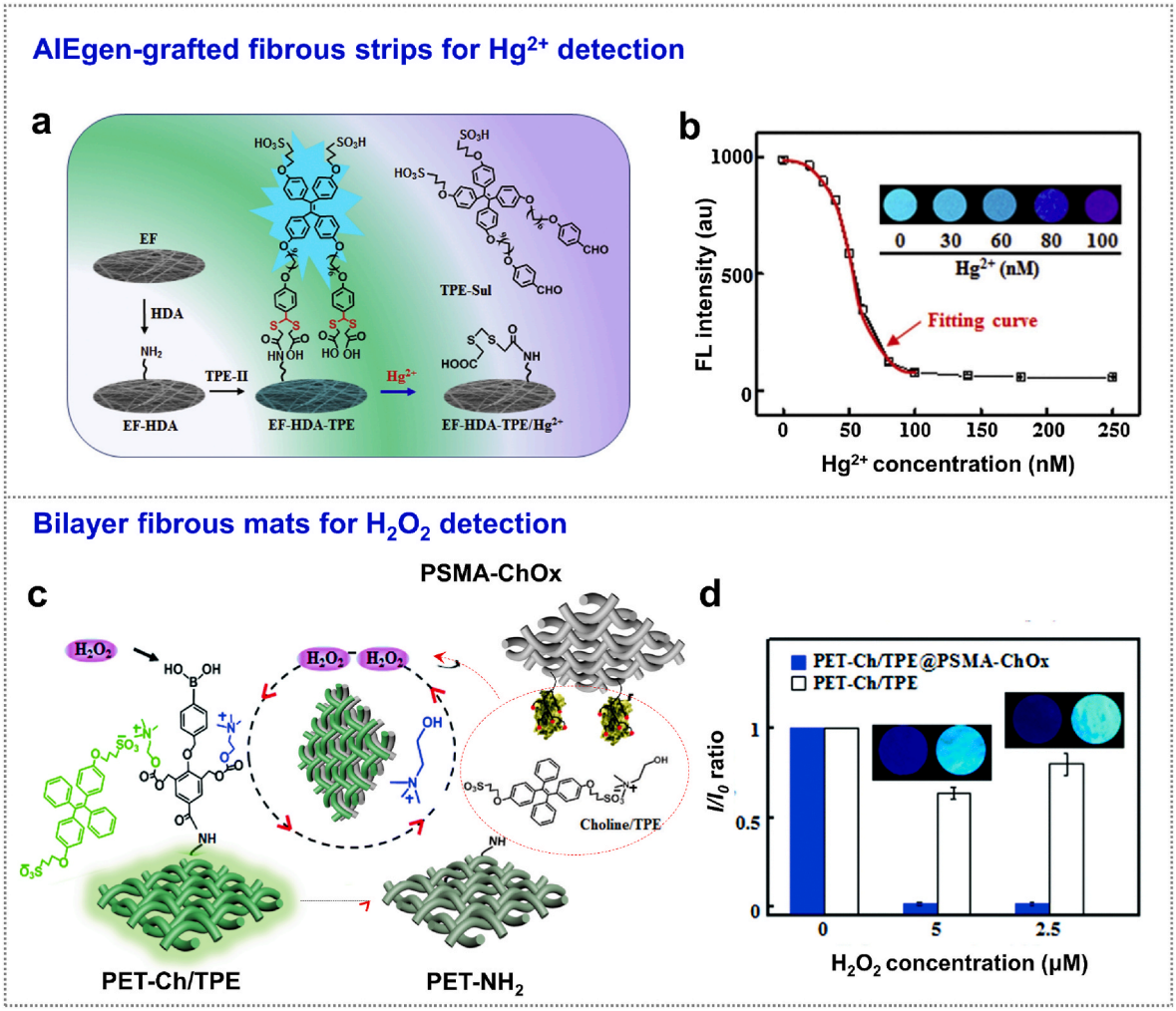

Fig. 3. Metal ions and H_2O_2 detection. (a) TPE derivatives-grafted fibrous strip for Hg^{2+} detection. (b) The fitting relationship between emission intensity of the fibrous sensor and Hg^{2+} levels. Inset: The color of fibrous strips in response to different levels of Hg^{2+} under 365 nm UV light. Adapted with permission from Ref. [40]. Copyright 2019 Elsevier. (c) Bilayer fibrous mats (PET-Ch/TPE@PSMA-ChOX) for H_2O_2 and choline sensing. (d) The signal amplification by introduction of choline oxidase layer (PSMA-ChOX). Insets showing the corresponding fluorescence fading in response to H_2O_2 concentration (365 nm irradiation). Adapted and reproduced with permission from Ref. [32]. Copyright 2019 The Royal Society of Chemistry. (For interpretation of the references to color in this figure legend, the reader is referred to the Web version of this article.)

limit of detection (LOD) was demonstrated as low as 20 nM, fulfilling the threshold concentrations in drinking water. This strategy could be further applied for other small molecules detection by decorating with a suitable recognition unit. For example, Li et al. developed a visual sensor of hydrogen peroxide (H_2O_2) and choline by integration of double-layer nanofibrous film [32] (Fig. 3c). On the visual sensing side of the film, the probes composed of phenylboronic acid and choline units were grafted on the PET-Ch/TPE nanofibrous film, followed by electrostatic adsorption of sulfonated-TPE to form fluorescent fibers; on another side, choline oxidase was immobilized on PSMA-ChOX nanofibers. The presence of H_2O_2 initiated the cleavage of the probes to release choline and choline/TPE complexes from nanofibers. The released choline was again captured by choline oxidase to generate H_2O_2 that further activated the cleavage reaction until release all choline/TPE complexes, leading to sensitive detection of bioactive H_2O_2 in a "turn-off" way (Fig. 3d). In this process, the signals of the probe were in situ amplified by choline oxidase, showing a LOD of 0.5 μM H_2O_2. The trace analysis of H_2O_2 is valuable toward the early diagnosis of disease, because its excessive presence normally leads to cancer, cardiovascular diseases, and inflammation. This double-layer fibrous sensor integrated a sensing layer and an amplifier layer in one material, simplifying the sensing process and providing potential to screen trace levels of biotargets, even in resource-constrained settings.

Glucose serves important role in carbohydrate metabolism, whose level in the blood and urine is related to the human health because abnormal levels of glucose will lead to diabetes mellitus [55,56]. Generally, glucose measurements are based on interactions with glucose oxidase, which is the standard enzyme for biosensors for glucose detection. The biosensing mechanism is known by the enzyme catalysis of glucose to formation of H_2O_2 [57]. Compared with instrumental analysis systems, colorimetry/fluorometry glycosuria test strips are easy-visualized and cost-effective, benefitting for family and individual self-testing [58–60]. Chao et al. designed poly (amic acid) (PEBA) bearing AIE units and oligoaniline segments, which was utilized as a dual-response sensor (colorimetric and fluorometric) followed by electrospinning (combined with PAN) (Fig. 4a) [54]. Redox reaction was occurred between oligoaniline and generated H_2O_2 by glucose oxidase, resulting in obvious color change from gray to yellow-green in appearance. During this process, oligoaniline segments could be transformed into emeraldine base (EB) or pernigraniline base (PNB), showing obvious absorption enhancement in the visible range. Simultaneously, its fluorescence was quenched gradually because of the energy transfer between the oxidized quinone of the oligoaniline segments and the excited state of the AIE units in PEBA (Fig. 4b and c). In this design, dual-mode glycosuria visual detection was highly desirable, which could reduce intuitive judgment errors (Fig. 4c). The fibrous device is also reusable after the reduction process by the treatment in hydrazine hydrate solution. In addition, the large specific surface area of the nanofibrous membrane endowed highly efficient interaction with analyte, showing higher sensitivity compared with referenced commercial test strips.

The sensing of water vapor generated by the evaporation of perspiration from the skin and exhaled moisture has applications in medical diagnostics [62,63]. Different from the previous examples that focusing

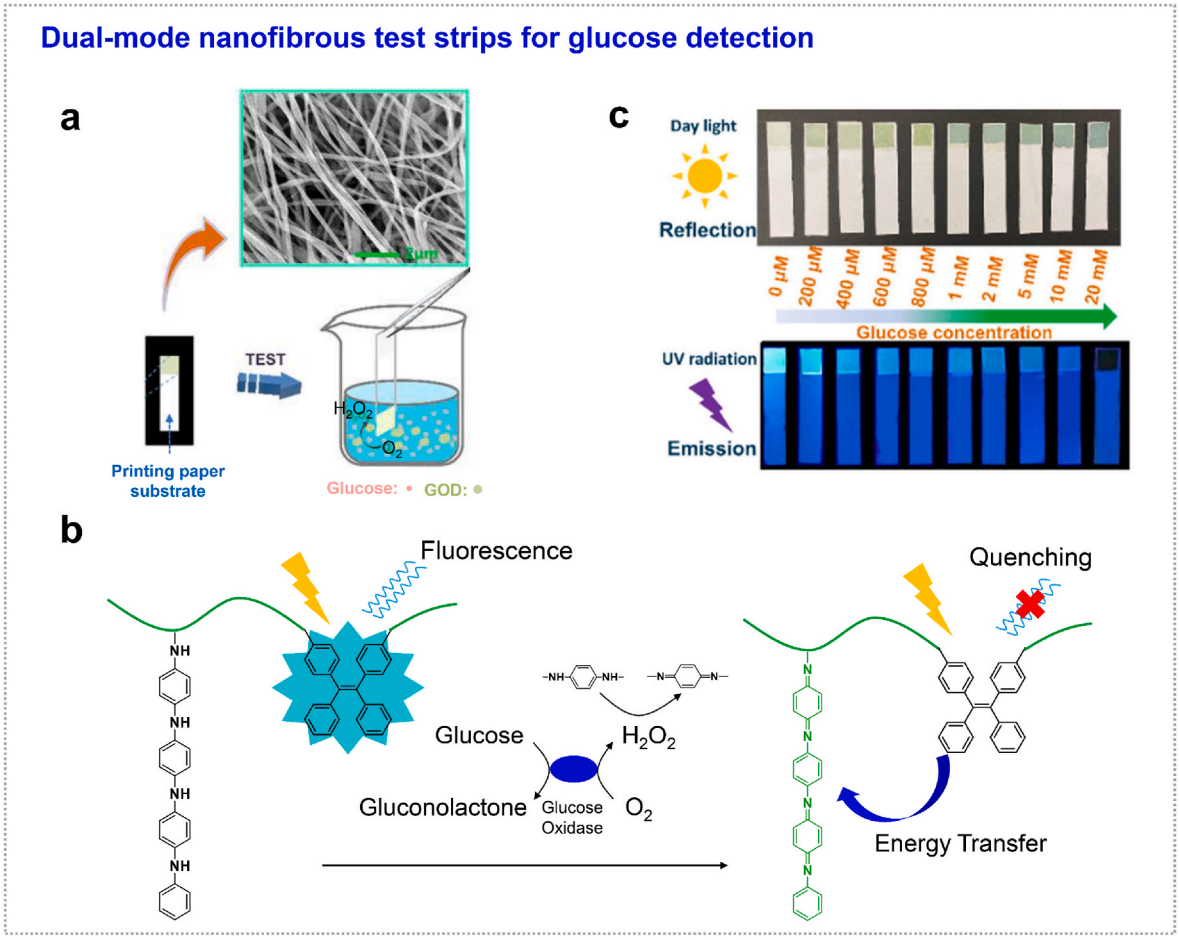

Fig. 4. Glucose detection. (a) AIE-PEBA-PAN fibrous test strip for glucose testing. (b) Mechanism of colorimetric and fluorometric dual-response sensor. (c) Dual-mode of colorimetric and fluorometric visual glycosuria sensing at different glucose concentrations. Images taken under daylight and UV radiation, respectively. Adapted and reproduced with permission from Ref. [54]. Copyright 2021 Elsevier.

on the emission intensity, developing a water-vapor sensor showing multicolor response would be very rewarding. Tang et al. utilized AIE-active molecular rotors (TPE-Py) as a fluorescent sensor, which is characterized with twisted intramolecular charge transfer (TICT) effect [61]. Its emission is highly dependent on surrounding polarity due to the donor-acceptor structures. They incorporated TPE-Py into water-captured network of polyacrylic acid (PAA), then used electrospinning method to obtain nanofibrous film (Fig. 5a). Due to the high-water absorptivity of PAA network, the emission color of the film changed from blue to orange when the relative humidity increased from 0% to 99% (Fig. 5b). Their emission maximum versus relative humidity could be fitted to a linear relationship, accounting for quantitative and precise water vapor measurement. Benefitting from the large surface area of nanofibrous film, the film could response human exhalation and recovered to the original state within 1 s (Fig. 5c). Besides this, the nanofibrous film was demonstrated for fingerprint mapping. After direct contact of fingertips with substrate, nonpolar sweat components (oil, grease) on finger ridges were left to act as a hydrophobic layer to screen the surfaces from interacting with water vapor, allowing a clear visualization of the ridges (blue emission) and valleys (yellow emission). Meanwhile, the sweat pores also appeared because of the dissolution of the fibrous film (Fig. 5d). This multicolor visualization technology shows advantage since the fluorescence intensity-based "turn-on" and "turn-off" detection are sensitive to the excitation power and the detector sensitivity. It would offer opportunities for applications in clinical diagnosis, information security protection, and human-machine interaction.

Proteins. Alkaline phosphatase (ALP) is an enzyme that is found throughout the body, especially concentrated in the liver, bones, and digestive system [66,67]. Abnormal level of ALP in the blood indicates liver or bone disorders [68,69]. Therefore, in situ monitoring the ALP activity is important for biomedical researches and clinical diagnoses. Compared to "turn-on" or "turn-off" strategies that traditional fluorescence ALP detection used, a ratiometric method based on the ratio of two fluorescence emissions exhibits great advantages, avoiding the susceptibility from the single-emission intensity changes [70]. Li et al. developed a ratiometric analysis of ALP activity by covalent grafting fluorescein (green emission) onto electrospun polyethylene terephthalate (PET) nanofibers [64], and then further binding with bis-quaternary ammonium salt of tetraphenylethene (TPE-$2N^+$, blue emission) through electrostatic interaction (Fig. 6a). The as-prepared nanofibrous membrane showed the emission of TPE-$2N^+$ at 471 nm, while the emission of phosphorylated fluorescein was suppressed. In the presence of ALP, the phosphate groups were removed after phosphoester hydrolysis, resulting in the release of TPE-$2N^+$ to reduce the emission at 471 nm and the restoration of fluorescein emission at 514 nm. With increasing ALP concentrations, the ratiometric fluorescence responses of fibrous strip resulted in color changes from blue to green accordingly (Fig. 6b) This ALP detection was demonstrated to show no apparent interference by serum components, and exhibited a straight visual detection of ALP levels (0–80 mU/mL) in human serum.

This ratiometric strategy was further applied in the detection of heparin and trypsin based on the bifluorophoric system that grafted on fibrous strips. As shown in Fig. 6c, a TPE derivative with sulfonated unit and phloxine B (PhB) were covalently immobilized on PSMA nanofibers [65], then protamine adsorption was followed to quench the emission of PhB (yellow, 574 nm) and then induced the emission of sulfonated TPE (green, 472 nm). The presence of heparin or trypsin removed protamine to restore the fluorescence of PhB but relieved the emission of the sulfonated TPE (good water solubility). As a result, the ratiometric detection of heparin and trypsin was achieved by using the fluorescence-intensity ratio of I_{574}/I_{472}. This fibrous strip provides the potential for facile and visual monitoring serum heparin and urine trypsin levels during long-term care of patients (Fig. 6d and e). In above examples, the authors modified AIE-based probes with targeting ligands, allowing specifically recognition through a lock-and-key interaction.

Bacteria. Pathogenic microbes (such as *E. coli*) can cause infections or diseases in human body [73]. Therefore, detection of the microbe levels in water and biological fluids is important for water and food safety, environmental monitoring, and clinical diagnosis [74–76]. Although polymerase chain reaction (PCR)-based methods guarantee the high accuracy of microbial detection, they suffer from sophisticated

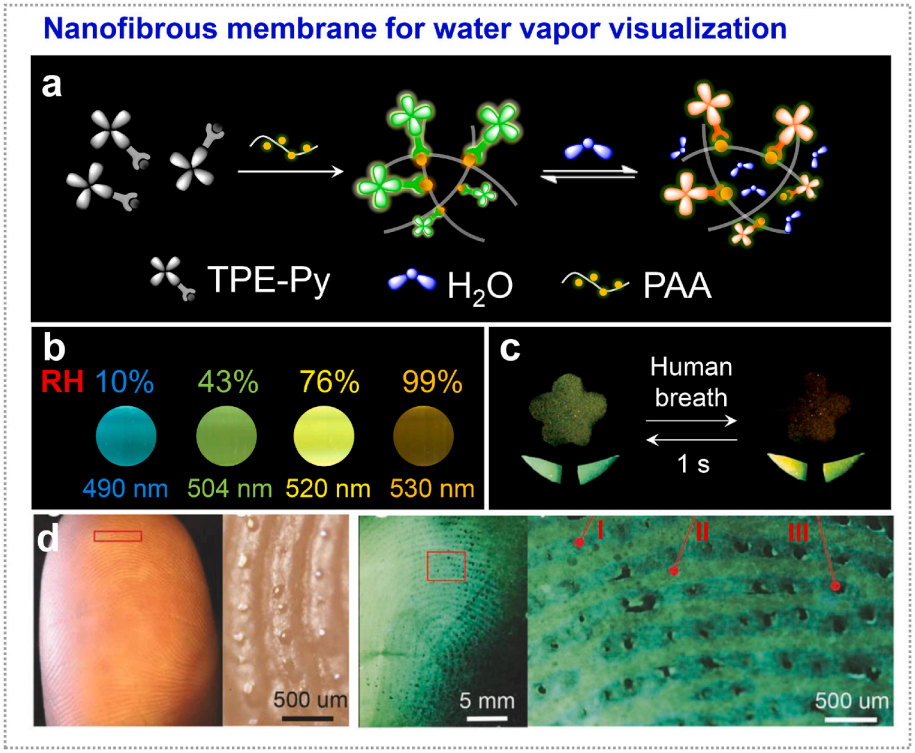

Fig. 5. Water vapor detection. (a) Design of TPE-Py-doped polyacrylic acid (PAA) nanofibrous fluorescence sensors for water vapor visualization. (b) The fluorescence colors of TPE-Py-PAA film upon the relative humidity increasing from 0% to 99%. (c) Reversible and rapid response of nanofibrous film in a flower pattern (flower leaves: TPE-Py-PAA) to human exhalation. Photos taken under 365 nm UV irradiation. (d) The photos of the finger pulp and fingerprint mapping on the TPE-Py fibrous membrane. In the rightmost magnified image, the alternate blue and yellow lines correspond to the ridges (I) and valleys (II) of fingerprint, while the black points correspond to the sweat pores (III). Adapted and reproduced with permission from Ref. [61]. Copyright 2017 Wiley-VCH Verlag GmbH & Co. (For interpretation of the references to color in this figure legend, the reader is referred to the Web version of this article.)

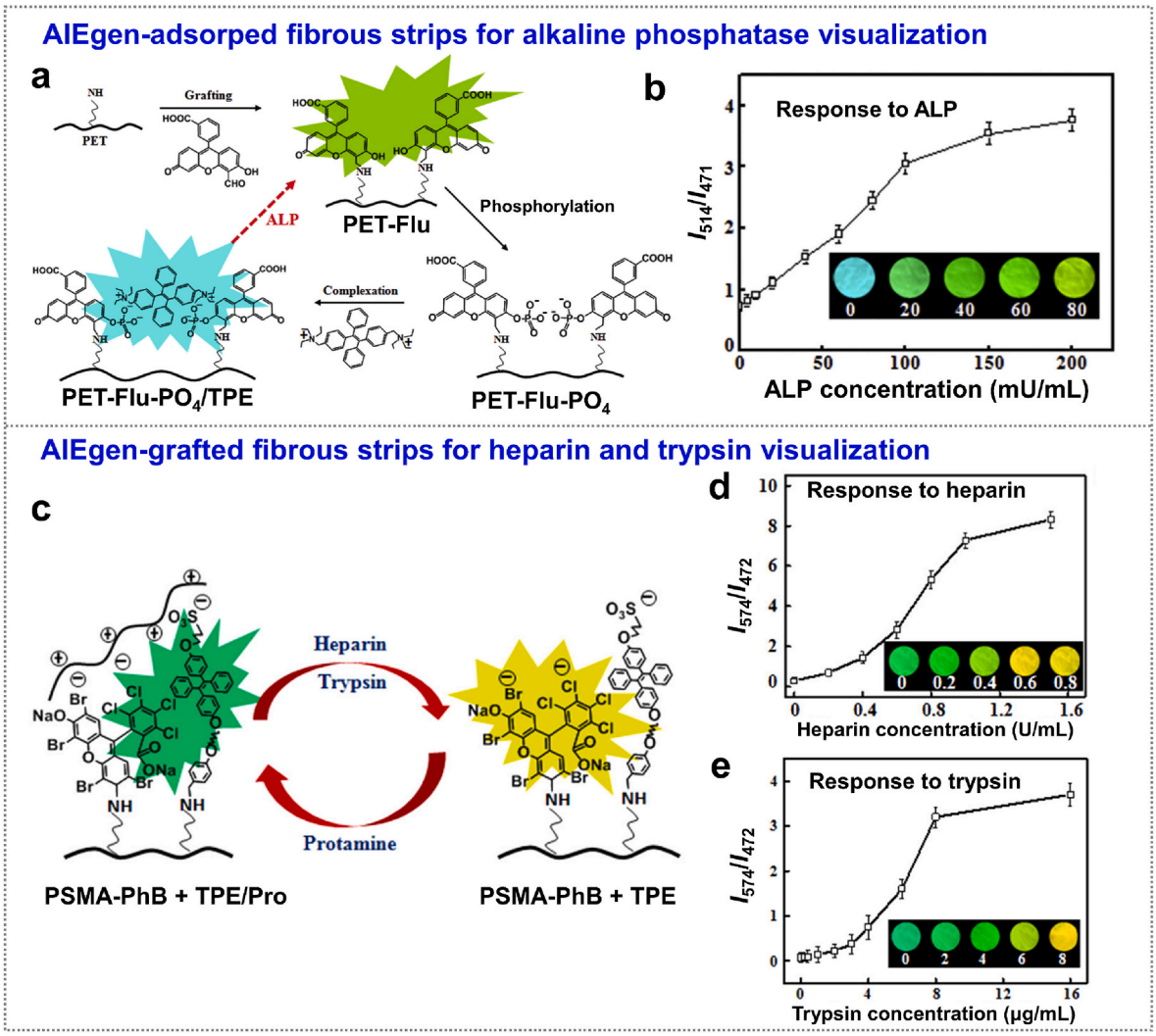

Fig. 6. Proteins detection. (a) Ratiometric fluorescence sensors for the detection of ALP. Schematic illustration of fluorescein carbaldehyde grafting, fluorescein phosphorylation, and electrostatic complexation of TPE-$2N^+$. (b) I_{514}/I_{471} ratios of fibrous mats in the presence of ALP at different concentrations, the insets are the corresponding fluorescence images of the strips irradiated under 365 nm UV light. Adapted and reproduced with permission from Ref. [64]. Copyright 2016 Elsevier. (c) Schematic illustration of the ratiometric color changes of fibrous sensor. The sensing of heparin or trypsin was occurred by removing the adsorbed protamine. (d, e) I_{574}/I_{472} ratios of the fibrous sensor at different concentrations of (d) heparin and (e) trypsin, the insets are the corresponding fluorescence images of the strips under 365 nm UV light. Adapted and reproduced with permission from Ref. [65]. Copyright 2017 American Chemical Society. (For interpretation of the references to color in this figure legend, the reader is referred to the Web version of this article.)

instrumentations and complicated procedures to obtain results [77]. The combination of fluorescence technology and electrospun fibrous strip provides ultrafast, visualized and on-site detection of microbes [78]. In addition to a high availability of graft sites for fluorescent recognition provided by the fibrous sensors that discussed above, the open and entangled porous fibrous networks endowed it with rapid interception capability for microbes [79]. Although an electrostatic interaction was applied to binding with various bacteria (negatively charged surface) by introducing positively charged group into AIEgens, which was not appropriate for specific targeting and labeling. Fortunately, the surface of bacteria offers specific sites to recognize and bind for AIE probes through a recognition interaction. It is well acknowledged that *E. coli* utilize the interactions between bacterial fimbria and mannose moieties from the host cell surface to establish infections in host [80]. At the end of a fimbria, FimH proteins are usually exploited for an effective detection based on its sugar-binding properties. In this case, TPE was functionalized with mannose units (TPE-Man) that can specifically interact with FimH in a fast and sensitive manner. Li et al. grafted TPE-Man on electrospun fibers for *E. coli* detection in aqueous solution (Fig. 7a) [71]. TPE-Man conjugated on nanofibers was not emissive in aqueous solution because of their good water solubility. Due to the existence of poly (ethylene glycol) chains between AIE probes and fiber matrices, the intramolecular motions of TPE-mannose on the surface were activated to show weak emission at the initial state. A specific interaction between mannose group and *E. coli* resulted in the intramolecular motion restriction of the TPE unit and then generated strong emission in the "turn-on" mode, which is in contrast to the ion detection that showing strong emission at the beginning state (Fig. 3a). Such fibrous sensors enabled specific, visualized and quantified detection of *E. coli* with a detection limit of 10^2 CFU/mL.

Compared with static sensing of *E. coli* by fibrous strip sensors, moving fiber-rod-based micromotors were designed to exhibit a higher sensitivity because of motion-enhanced bacteria caption. Janus fiber rods constitute of two sides: one side was grafted with TPEC-Man to lighting *E. coli*, another side was decorated with catalase to decompose H_2O_2 fuel into oxygen bubbles for pushing the movement of Janus fiber rods (Fig. 7b). The authors named this strategy as "motion-capture-lighting", which integrated the capability of motion-enhanced capture

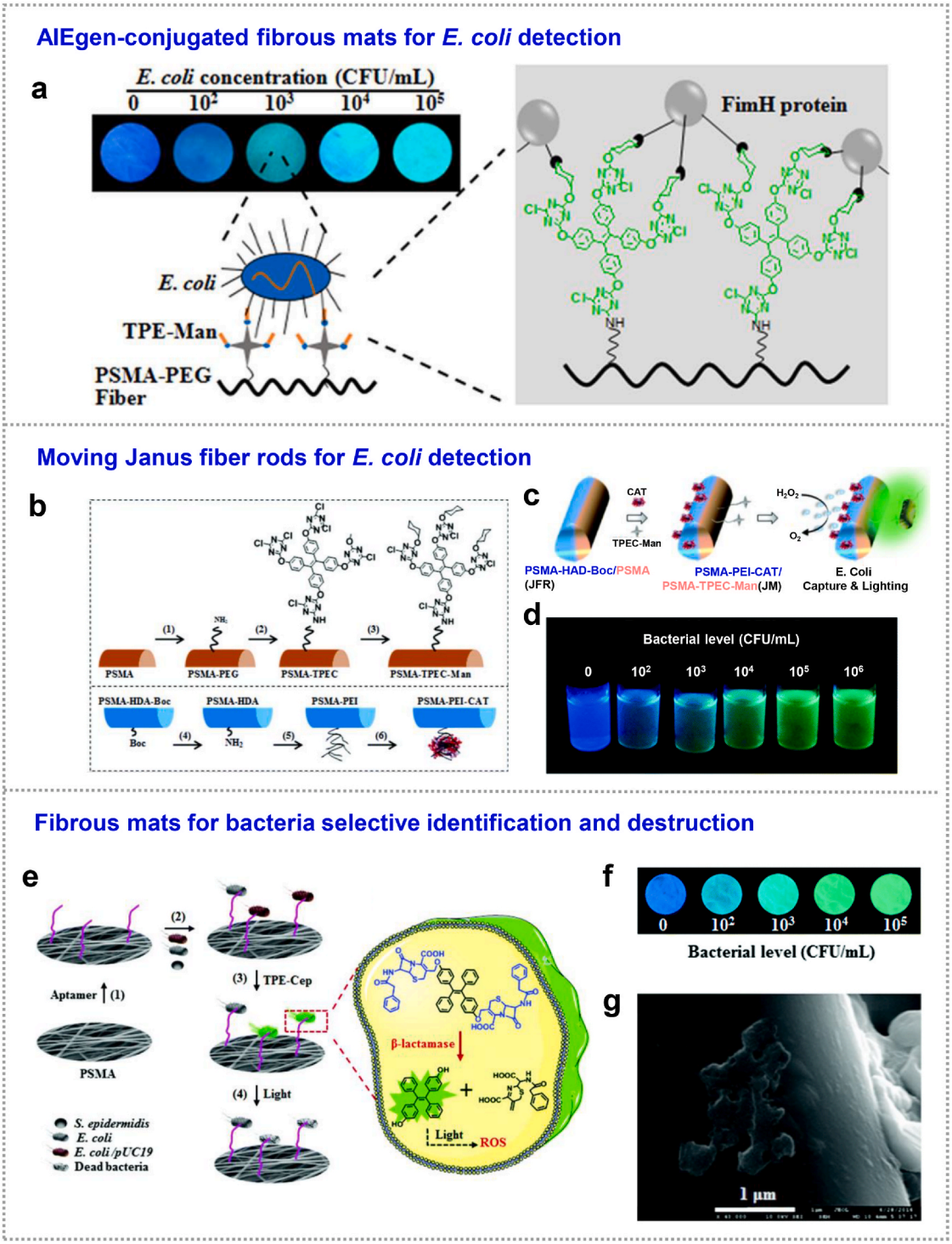

Fig. 7. Bacteria detection. (a) (left) TPE-Man-grafted PSMA-PEG nanofibrous sensor for *E. coli* detection and (right) the corresponding working mechanism. The fluorescence images showing the enhanced emission with an increase in *E. coli* concentration. Adapted and reproduced with permission from Ref. [71]. Copyright 2015 American Chemical Society. (b) Schematic illustration of specific grafting on two sides of Janus fiber rods. One side was grafted with AIE probes of TPEC-mannose, the other was conjugated with catalase to react with H_2O_2 for propelling fiber rods. (c) Fluorescence response of Janus micromotors after binding with *E. coli*. The decomposition of H_2O_2 fuels by catalase provided the propulsion force to enhance the specific binding between mannose moieties and *E. coli*, which initiated the AIE effect of TPE units and then "turn-on" the fluorescence of fiber rods. (d) Fluorescence photographs of Janus fiber rods suspensions at different *E. coli.* concentrations. Adapted and reproduced with permission from Ref. [33]. Copyright 2019 The Royal Society of Chemistry. (e) Schematic illustration of bacterial capture and destruction on fibrous mats modified by aptamer and then TPE-Cep. (f) Fluorescence images of fibrous color strips incubated with *E. coli/pUC19* at various concentrations taken under 365 nm UV light. (g) SEM image of the destroyed structure of the captured bacteria on the surface of fiber. Adapted with permission from Ref. [72]. Copyright 2020 The Royal Society of Chemistry. (For interpretation of the references to color in this figure legend, the reader is referred to the Web version of this article.)

of bacteria and capture-induced fluorescence "turn-on" of micromotors (Fig. 7c and d) [33]. Compared with the static sensing by fibrous strips discussed above, the sensitivity of moving micromotors could be enhanced with lower LOD by low-fold.

Owing to the overuse of antibiotics in food industry and medicine, differentiating antibiotic-resistant bacteria from normal ones is another urgent challenge in environmental control and human healthcare [81]. Visual evaluation of antibiotic resistance provides a fast and direct observation of antibiotic-resistant bacteria. β-lactamases is widely used to disrupt the antibiotic activities of bacteria, and is behaved as an important marker for screening of resistant bacteria [82,83]. The major challenge is how to combine of specific strains isolation, a low level of resistant bacteria sensing, and killing capability in one system. Li et al. developed a fibrous sensor that was integrated with capture ligands and then AIE probes to achieve selective identification and simultaneous killing drug-resistant bacteria (Fig. 7e) [72]. Specifically, aptamer ligands were firstly conjugated on nanofibers for specific bacterial capture. Water soluble AIE probes with TPE cores and two terminal cephalosporin molecules (TPE-Cep) were constructed for recognizing and destroying antibiotic-resistant strains. TPE-Cep probes could only be cleaved by endogenous β-lactamases in resistant bacteria, yielding water-insoluble TPE derivative aggregates of TPE-OH and then emitted fluorescence immediately (Fig. 7f). In addition, the released TPE-OH could serve as a photosensitizer (PS) to produce ROS for destroying bacteria at some extent under light illumination (even though not high). As shown in Fig. 7g, collapsed and fusion of bacteria were observed on the fiber surface. Such an integrated sensor was demonstrated to show multiple functions toward simultaneous quantitative visualization and image-guided photodynamic ablation of antibiotic-resistant bacteria.

Fibrous aggregates, especially nanofibrous networks, provide powerful matrices or substrates in sensing biomolecules with high specificity, selectivity and visibility. AIE probes were embedded in polymer matrix of fibers or grafted onto the surface of fibers to interact with analytes for sensing, representing an effective strategy for separations from water or biological fluids, and avoiding consuming sample post-treatment. The generated fluorescence signals were expressed out in turn-on, turn-off or multicolor modes. Strategies such as reaction-mediated, binding-mediated, and cleavage-mediated were achieved through smart integration of AIE probes and fiber structures. In the future, the development of "AIE + Fiber" sensors could be achieved by the decoration of more recognition moieties in AIE probes, architecture design of fibers, performing clinical sample testing, and device assembling for healthcare monitoring. Most recently, optical fibrous devices have been demonstrated to show their advantages in SARS-CoV-2 detection because of their remote signal transfer capability, which could be used for patients in remote areas without hospitals or clinical laboratories [84,85]. On the basis of the developed AIE probes that have been applied in nucleic acid detection and immunological assays [86,87], we believe the combination of optical fibers and AIE probes have high potential for reliable COVID-19 screening in some specific application scenarios.

3. Therapy

AIEgens could not only allow visualization of biotargets existence and monitoring their concentration, but also provide therapeutic functions like photodynamic therapy and photothermal therapy for various diseases [88]. Biosensing mechanisms of AIEgens focused on the exploitation of radiative energy of fluorescence, while therapeutic functions of AIEgens are developed by harnessing the energy of non-radiative pathways [89]. For photosensitizers (PSs), upon excitation, they could undergo intersystem crossing to the triplet state and further react with the surrounding oxygen to generate ROS [19]. ROS (highly toxic) can kill bacteria or destroy disease tissues but also constrain the damage to microbes or cancer cells, owing to its short radius and life time [90,91]. Therefore, PSs involved photodynamic therapy is considered as a noninvasive and effective treatment modality [92]. For photothermal agents, by introducing molecular rotors and flexible alkyl chains to the planar skeletons, the intramolecular motions are activated and thus the nonradiative decay could be further improved, affording high efficient photothermal conversion and photothermal therapy [93]. Photothermal therapy is an extension of photodynamic therapy, which is able to use longer wavelength light thus requires less energy and shows less harmful to other cells and tissues [94].

In contrast to traditional PSs that usually undergo self-quenching in aggregates via nonradiative decay, AIE-active ones show low non-radiative decay and exhibit enhanced emission and photosensitization [97,98]. Taking advantage of the unique properties of AIE-active PSs, incorporating them into polymer fibers could further increase the ROS generation because of the physical confinement provided by polymer matrix. In addition, compared with those of planer materials, fibers offer abundant high-surface area to fully contact with oxygen for sustaining high ROS production. Most importantly, the fibrous carriers broaden the application scope of AIEgens and make them more practicality. Triggered by these advantages, Tang et al. incorporated a photosensitizer of TBP into poly (ε-caprolactone) (PCL) nanofibers by a hand-held electrospinning device as shown in Fig. 8a [95]. In previous study, cationization of PSs has been demonstrated to be an attractive way to enhance photodynamic therapy, due to the specifically targeting the cancer cells and bacteria/electron-negative viruses surface [6,19]. The obtained nanofibrous membrane was applied as wound dressings and characterized with following advantages: high surface area-enhanced damaged tissues contact, high porosity-allowed air permeability, biomimetic extracellular matrix-induced healing at molecular level, and antibacterial activity provided by TBP (Fig. 8b and c). Compared with traditional gauze, this photodynamic-boosted antibacterial wound dressings assisted by handheld electrospinning show highly potential for treating emergencies, such as military injuries.

Since the discovery of SARS-CoV-2, hundreds of millions of people infection and millions of deaths are caused worldwide [87,99]. Because the coronavirus is mainly transmitted through droplet and aerosol, personal protective equipment (such as facemasks) is still considered the most effective way to intercept microbe and protect individuals from COVID-19 infection [100,101]. The multilayer fibrous structure of facemasks has been demonstrated to capture or filter the viruses particles [102], allowing comfortable breathability for longer durations. However, arbitrarily discarding and inappropriate disposal of personal protective equipment may cause a high risk for cross-contamination [100,103]. Recently reported self-sterilizing masks mediated by photodynamic and photothermal therapies show great potential to address above problems.

Huang et al. attached an efficient AIE-active PSs (ASCP-TPA) on fabrics of personal protective equipment (*e.g.*, white gown, surgical mask, N95 mask), endowing fabrics with photodynamic-mediated virucidal and self-sterilizing capabilities (Fig. 8d) [96]. The broad absorption spectrum of ASCP-TPA indicated the possibility for ROS generation by white light. ASCP-TPA-attached fabrics (ATaFs) were obtained by simply immersion (ASCP-TPA solution), squeezing, and solvent evaporation process. Upon attachment on the surface of polymer fibers, AIEgen of ASCP-TPA showed strong emission due to the restriction of intramolecular motion, leading to high ROS production. In addition, the positively charged pyridinium unit of ASCP-TPA makes it possible to attract negatively charged viruses and virus-containing respiration droplets, promoting the photodynamic inactivation effect when viruses reach the surface of ATaFs. They demonstrated that >99.999% virions on the ATaFs were eliminated within 10 min even irradiated under ultralow power (3.0 mW/cm^2) (Fig. 8e). The ASCP-TPA-attached fiber strategy endows personal protective equipment with rapid virus-killing ability and ultralow-energy consumption, affording real-time protection even under indoor light irradiation. Surprisingly, no obvious AIEgens leaching from the ATaFs was proved by absorption spectra after washing 100 times, demonstrating the modified

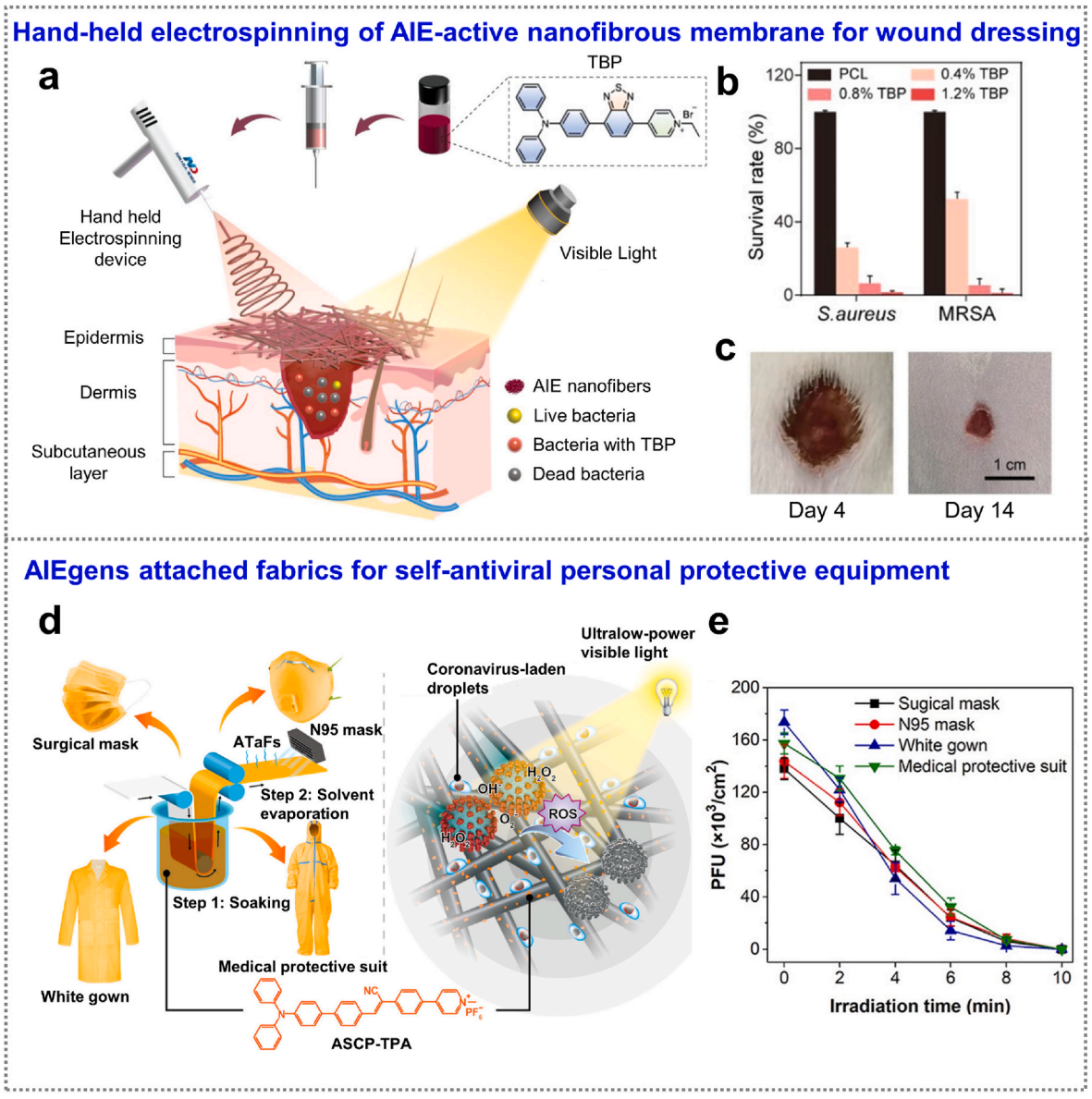

Fig. 8. Photodynamic therapy. (a) Schematic illustration of hand-held electrospinning of TBP-incorporated antimicrobial dressing. (b) Antibacterial activity of the nanofibrous membrane with various TBP concentrations. (c) Healing ability of the nanofibrous wound dressing. Adapted with permission from Ref. [95]. Copyright 2022 Wiley-VCH Verlag GmbH & Co. (d) Schematic illustration of the construction of ATaFs and the photodynamic inactivation of the coronavirus. (e) Virucidal effects of four kinds of ATaFs (irradiation density: 3.0 mW cm^{-2}). Adapted with permission from Ref. [96]. Copyright 2021 American Chemical Society.

ATaFs with long-term usability and washability. In addition, long-term and high-power irradiation applied to ATaFs indicated no toxicity to normal skin. Such simple combination of AIE-active photosensitizers and fabrics provides a simple but effective strategy to fight against airbone pathogens and coronavirus.

Generally, D-A structured AIEgens are potential to exhibit simultaneous photodynamic and photothermal functions from balanced energy dissipation. On one hand, narrow HOMO-LUMO bandgap facilitates AIEgen with enhanced absorption in near-infrared (NIR) region to dissipate excited-state energy through nonradiative decay and thus generates heat [93], while D-A structures show separated HOMO–LUMO distribution and reduce ΔE_{ST} to transform triplet-state energy into chemical energy of ROS for photodynamic therapy [92,106]. It also has been proved that the ISC process could be further enhanced by incorporating AIEgens in the rigid matrix, because the phenomenon of aggregation-induced generation of ROS [107]. Besides, through elaborated molecular engineering, the nonradiative thermal dissipation could be strengthened by promoting intramolecular motion of D-A structured AIEgens. Photodynamic and photothermal treatment could be simultaneously utilized by making full use of ROS and heat [17]. AIEgen of TTVB exactly falls into this category. Wang et al. incorporated this molecule into poly (vinylidene fluoride-*co*-hexafluoropropylene) (PVDF-HFP), electrospinning technique was followed to obtain nanofibrous membrane (TTVB@NM) as shown in Fig. 9a [104]. Upon sunlight irradiation, TTVB@NM could produce massive ROS and moderate photothermal conversion properties, exhibiting photodynamic and photothermal broad-spectrum inactivation of bacteria (inhibition rate: >99%), fungi (~88%), and viruses (>99%) (Fig. 9b). Using the similar strategy, they utilized a D-A-D molecule of TPA-BTDH (an NIR-II dye) to dope into poly (methyl methacrylate) (PMMA) nanofibrous aerogel (Fig. 9c) [105], the resulted aerogel also showed both photothermal conversion and ROS production. The 3D aerogel possesses interconnected micro/nano pore structure, which could inhibit the light reflection/scattering to achieve high light absorption and high photothermal conversion performance [34]. Such aerogel was demonstrated to play as water evaporator for water purification, the generated heat

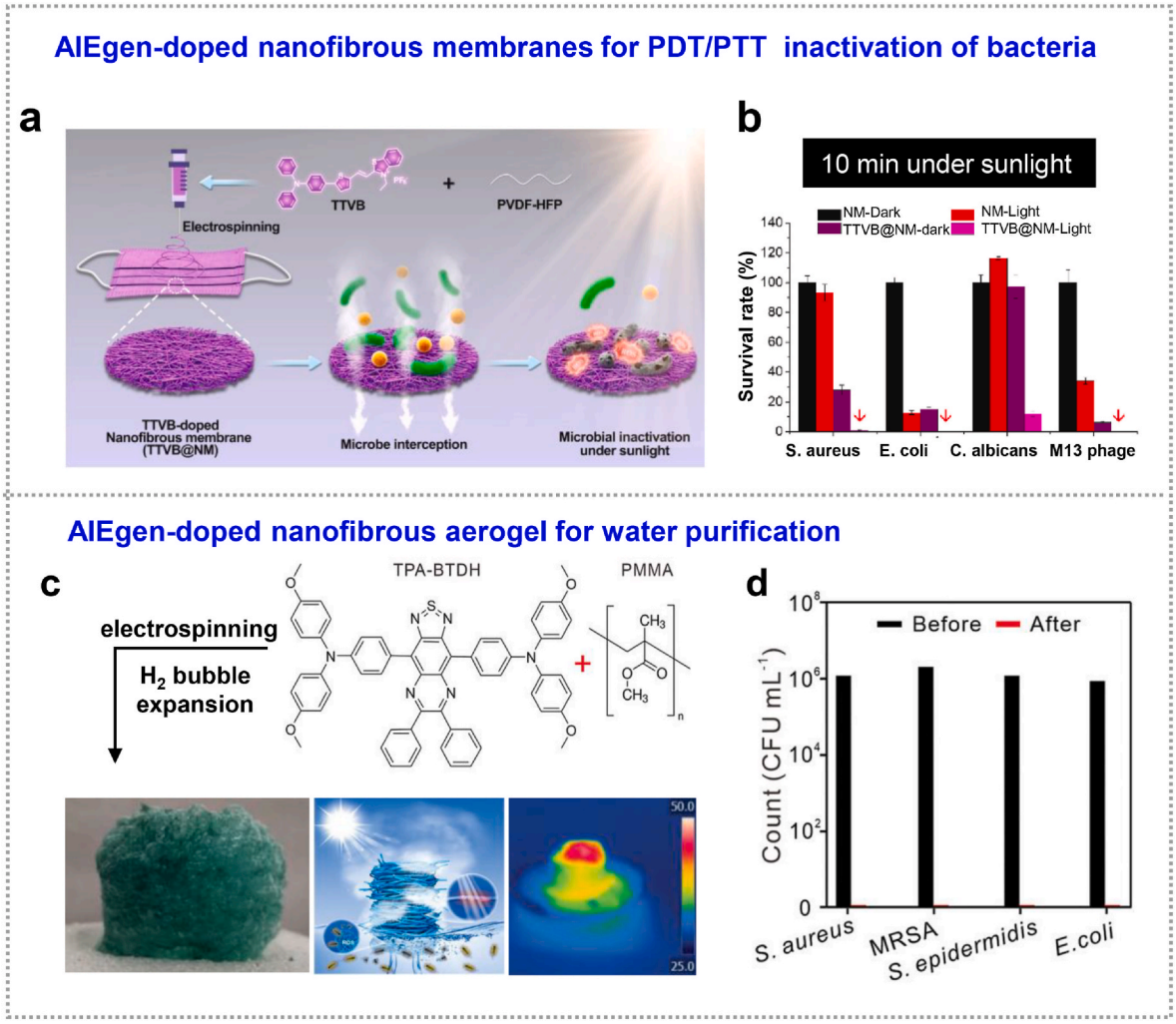

Fig. 9. Combined photodynamic and photothermal therapy. (a) Schematic illustration of the electrospinning of nanofibrous membrane TTVB@NM and its inactivation of bacteria, fungi and viruses upon sunlight irradiation. (b) Survival rates of different microbes after 10 min sunbathing. Adapted with permission from Ref. [104]. Copyright 2021 Elsevier. (c) Preparation and photograph of TPA-BTDH-doped fibrous foam, and their water purification mechanism. (d) The counts of bacterial clones in the simulated wastewater before and after water evaporation. Adapted and reproduced with permission from Ref. [105]. Copyright 2021 Wiley-VCH Verlag GmbH & Co.

and ROS from embedded TPA-BTDH were utilized for evaporating water and killing the bacterial nearby the fiber (Fig. 9d), endowing the aerogel evaporator with antibiofouling behavior. However, in both examples, although the ROS production was benefitted from the balanced energy dissipations, the polymer matrix of fibers could inevitably restrict the intramolecular motion of AIEgens and thus reduced the photothermal efficiency.

Due to the twisted and rotor structure, restriction of intramolecular motion of AIEgens is commonly known mechanism to achieve high emission brightness [13]. If the molecular motion of AIEgens is activated, they can undergo nonradiative decay to dissipate their energy as heat [108], which is useful for photothermal therapy. Generally, the photothermal AIEgens are hydrophobic. Previous studies have been demonstrated that the plasticization of the alkyl chain is beneficial for molecular motion in the solid state to boost photothermal conversion [109]. However, molecular modification normally involves complicated synthetic routes and makes them difficult for large-scale application. Therefore, more advanced materials and technology are called for developing high photothermal efficient materials in a simple and effective way. In view of the above, Tang et al. developed a core-shell structure fiber by coaxial electrospinning, in which AIEgens containing oil as a core phase was stretched into the core layer of long fiber (Fig. 10 a and b) [35]. Evidently, the liquid oil could activate the molecular motion of the AIEgens, strengthening the nonradiative decay and then boosting photothermal efficiency. As shown in Fig. 10 c, the AIEgen of BPBBT embedded oil phase was served as the core phase and PVDF-HFP was played as shell layer. After 2 min of 1 solar irradiation, the temperature of such core-shell structured fibers (the BPBBT content = 0.6%) reached 56.1 °C, higher than those of directly doped nanofibers (40.4 °C). The photothermal conversion efficiency was calculated to be 22.36%, which is 26-fold as the homogeneous doping counterpart. The endurance of the core-shell structured fibers was also proved by cyclic irradiation, long-term storage, and washing tests. Under the natural sunlight, the temperature of the core-shell fibrous patch reached 51.2 °C after being covered on the knee of a volunteer (Fig. 10 d). The strong photothermal effect of this core-shell fibrous fabrics endowed them have a great potential in hot therapy and personal thermal management.

Fibers with functional additives are changing the way we think about the role of traditional fabrics, which provide an added benefit to the user beyond the typical value of the fabric. AIEgen as a superpower tool with photodynamic and photothermal capability could be introduced into fibers for biomedical protection. Meanwhile, fibers could be engineered with multiple components and special microstructures, offering various microenvironment to manipulate the aggregation state or

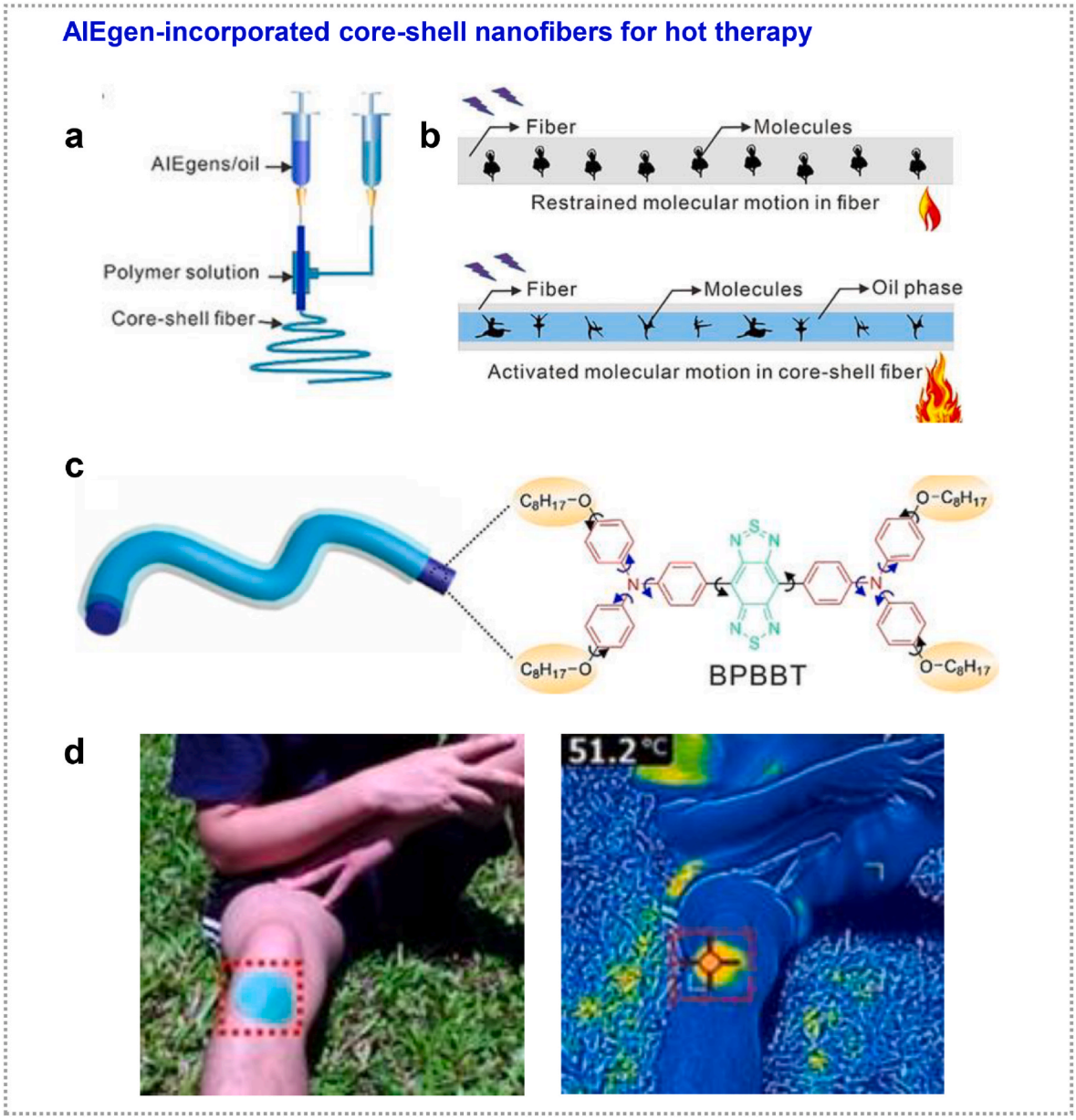

Fig. 10. Photothermal therapy. (a) Schematic illustration of coaxial electrospinning. (b) The restriction of intramolecular motion in polymer network of homogeneous fibers and the activation of intramolecular motion in oil phase of core-shell fiber. (c) Structure of a core–shell fiber and the activated molecular motion of BPBBT in oil phase. (d) The strong photothermal effect of the core-shell fibrous fabrics. Adapted with permission from Ref. [35]. Copyright 2020 Wiley-VCH Verlag GmbH & Co.

intramolecular motion of AIEgens thus to boost their ROS production or heat generation. The synergy of "AIE + Fiber" have been demonstrated to show high potential in wound dressings, self-sterilizing protection, and hot patches. Although remarkable progress, more fundamental studies are needed to fully elucidate the interaction between AIE-active molecules and polymer matrix, fiber structures, as well as entangled fibrous network and its influence on final performance.

4. Conclusion and perspectives

Over the past 20 years, great efforts have been made to develop various AIEgens through molecular engineering. Activated by the remarkable optical properties and therapeutic functions of AIEgens, a series of AIE probes with theranostic functions have been developed, which showing a great potential in biomedical applications. On the other hand, fibrous aggregates in forms of knitted or nonwoven fabrics have been widely adopted in medical textiles, including testing paper, protective apparel, surgical dressings and even implants. The right combination of "AIE + Fiber" is leading to better products that expand the boundaries of what's possible. The nearly limitless combination of chemical structures of AIEgens and advanced geometries of fibers allows characteristics such as biomolecular visualization, photosensitizing capability, and photothermal potential to be completely amplified (Fig. 11). Based on a series of representative examples, we disclose how AIE probes and fibers to be combined through the latest advances in biosensing and bioprotection, endowing AIEgens with improved functions for health protection and making them have potential to go beyond laboratory research.

Despite successful achievements in "AIE + Fiber" in the previous study, more efforts are still needed to be devoted to promote the progress:

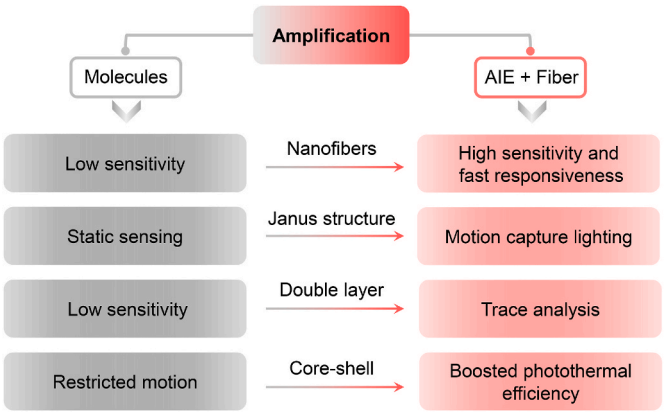

Fig. 11. Amplification effect of "AIE + Fiber" for biosensing and bioprotection.

(1) More fundamental researches are needed to elucidate the interaction between AIEgens and polymers at the molecular and mesoscale level, as well as its influence on final optical and therapeutic performance. The polymer chain structure, condensed microstructure, and spatial higher-order structure of the fibrous aggregates have preliminary been demonstrated to show effects on the aggregation states of AIEgens and then the optical properties. The fluorescent emission of AIEgens could be manipulated by the adjustment of their conformation and packing mode in polymer matrix of fibers. In addition, the photodynamic capability and photothermal conversion of AIEgens could also be further improved by polymer matrix design, which is worthy to be further explored.

(2) More fibrous structures could be developed and optimized for further improving the AIE performance, since the advanced engineering allows producing diverse structures in a single fiber (*e.g.*, porous, core-shell, hollow, Janus). For example, highly porous fibers could be introduced to combined with AIE probes for construction of fibrous sensors with improved sensitivity and responsibility, owing to the further increased surface area. Multicomponent fibrous system could be designed to endow AIEgens with abundant motion capability to improve photothermal conversion efficiency. In addition, AIEgen-incorporated fiber arrays with multi-target responses are also necessary, in which the probes synthesis and fiber design should be both considered.

(3) More functions, such as imaging, could be integrated in fibrous aggregates for health protection in vitro and in vivo. In vitro, the AIE probes for detection of microorganisms (*e.g.*, bacteria, viruses, fungi) could be integrated with fibrous personal protection equipment (*e.g.*, masks, protective suits), resulting in imaging the existence of microorganisms for personal protection. In vivo, NIR probes with long wavelength emission are more desirable for imaging, because of deep penetration, reduced photodamage, and high signal-to-noise characters. Fibers are widely used as degradable tissue scaffolds, the loss behavior is critical to evaluate their lifespan, mechanical strength, and mass transport characters. Assisted by NIR imaging technology, the degradation process could be visualized in situ, without extracting scaffolds once implanted in the body.

Credit author contribution statement

Z.Q., X.Y., J.Z., C.X., M.G., Y.C., and M.Z. participated in the discussion. Z.Q., X.Y., and Y.C. contributed to the writing of this paper.

Declaration of competing interest

The authors declare that they have no known competing financial interests or personal relationships that could have appeared to influence the work reported in this paper.

Data availability

Data will be made available on request.

Acknowledgement

This work was partially supported by the National Key Research and Development Program of China (2021YFA1201301/2021YFA1201300), National Natural Science Foundation of China (51973030, 52103075), Shanghai Rising-Star Program (20QA1400100), Science and Technology Commission of Shanghai Municipality (20JC1414900), the Fundamental Research Funds for the Central Universities, "DHU" Distinguished Young Professor Program (LZB2021001) and State Key Laboratory for Modification of Chemical Fibers and Polymer Materials, Donghua University.

References

[1] World Health Organization, United Nations Children's Fund, Water, Sanitation, Hygiene, and Waste Management for SARS-CoV-2, the Virus that Causes COVID-19: Interim Guidance, 29 July 2020, World Heal. Organ., 2020. https://apps.who.int/iris/handle/10665/333560.

[2] W. Fu, C. Yan, Z. Guo, J. Zhang, H. Zhang, H. Tian, W.-H. Zhu, Rational design of near-infrared aggregation-induced-emission-active probes: in situ mapping of amyloid-β plaques with ultrasensitivity and high-fidelity, J. Am. Chem. Soc. 141 (2019) 3171–3177, https://doi.org/10.1021/jacs.8b12820.

[3] Z. Pode, R. Peri-Naor, J.M. Georgeson, T. Ilani, V. Kiss, T. Unger, B. Markus, H. M. Barr, L. Motiei, D. Margulies, Protein recognition by a pattern-generating fluorescent molecular probe, Nat. Nanotechnol. 12 (2017) 1161–1168, https://doi.org/10.1038/nnano.2017.175.

[4] X. Han, R. Wang, X. Song, F. Yu, C. Lv, L. Chen, A mitochondrial-targeting near-infrared fluorescent probe for bioimaging and evaluating endogenous superoxide anion changes during ischemia/reperfusion injury, Biomaterials 156 (2018) 134–146, https://doi.org/10.1016/j.biomaterials.2017.11.039.

[5] H. Li, H. Kim, J. Han, V.-N. Nguyen, X. Peng, J. Yoon, Activity-based smart AIEgens for detection, bioimaging, and therapeutics: recent progress and outlook, Aggregate 2 (2021) e51, https://doi.org/10.1002/agt2.51.

[6] X. Shi, S.H.P. Sung, J.H.C. Chau, Y. Li, Z. Liu, R.T.K. Kwok, J. Liu, P. Xiao, J. Zhang, B. Liu, J.W.Y. Lam, B.Z. Tang, Killing G(+) or G(−) bacteria? The important role of molecular charge in AIE-active photosensitizers, Small Methods 4 (2020), 2000046, https://doi.org/10.1002/smtd.202000046.

[7] C.P.S. Ribeiro, L.M.O. Lourenço, Overview of cationic phthalocyanines for effective photoinactivation of pathogenic microorganisms, J. Photochem. Photobiol. C Photochem. Rev. 48 (2021), 100422, https://doi.org/10.1016/j.jphotochemrev.2021.100422.

[8] J. Kwon, S.W. Jun, S.I. Choi, X. Mao, J. Kim, E.K. Koh, Y.H. Kim, S.K. Kim, D. Y. Hwang, C.S. Kim, J. Lee, FeSe quantum dots for in vivo multiphoton biomedical imaging, Sci. Adv. 5 (2019), eaay0044, https://doi.org/10.1126/sciadv.aay0044.

[9] D.-Y. Zhang, Y. Zheng, H. Zhang, J.-H. Sun, C.-P. Tan, L. He, W. Zhang, L.-N. Ji, Z.-W. Mao, Delivery of phosphorescent anticancer iridium(III) complexes by polydopamine nanoparticles for targeted combined photothermal-chemotherapy and thermal/photoacoustic/lifetime imaging, Adv. Sci. 5 (2018), 1800581, https://doi.org/10.1002/advs.201800581.

[10] J. Li, Y. Liu, Y. Xu, L. Li, Y. Sun, W. Huang, Recent advances in the development of NIR-II organic emitters for biomedicine, Coord. Chem. Rev. 415 (2020), 213318, https://doi.org/10.1016/j.ccr.2020.213318.

[11] Z. Lei, X. Li, X. Luo, H. He, J. Zheng, X. Qian, Y. Yang, Bright, stable, and biocompatible organic fluorophores absorbing/emitting in the deep near-infrared spectral region, Angew. Chem. Int. Ed. 56 (2017) 2979–2983, https://doi.org/10.1002/anie.201612301.

[12] J. Mei, Y. Hong, J.W.Y. Lam, A. Qin, Y. Tang, B.Z. Tang, Aggregation-induced emission: the whole is more brilliant than the parts, Adv. Mater. 26 (2014) 5429–5479, https://doi.org/10.1002/adma.201401356.

[13] J. Mei, N.L.C. Leung, R.T.K. Kwok, J.W.Y. Lam, B.Z. Tang, Aggregation-induced emission: together we shine, united we soar, Chem. Rev. 115 (2015) 11718–11940, https://doi.org/10.1021/acs.chemrev.5b00263.

[14] W. He, T. Zhang, H. Bai, R.T.K. Kwok, J.W.Y. Lam, B.Z. Tang, Recent advances in aggregation-induced emission materials and their biomedical and healthcare applications, Adv. Healthc. Mater. 10 (2021), 2101055, https://doi.org/10.1002/adhm.202101055.

[15] C. Liu, H. Bai, B. He, X. He, J. Zhang, C. Chen, Y. Qiu, R. Hu, F. Zhao, Y. Zhang, W. He, J.H.C. Chau, S. Chen, J.W.Y. Lam, B.Z. Tang, Functionalization of silk by

AIEgens through facile bioconjugation: full-color fluorescence and long-term bioimaging, Angew. Chem. Int. Ed. 60 (2021) 12424–12430, https://doi.org/10.1002/anie.202015592.
[16] M. Gao, Y. Li, X. Chen, S. Li, L. Ren, B.Z. Tang, Aggregation-induced emission probe for light-up and in situ detection of calcium ions at high concentration, ACS Appl. Mater. Interfaces 10 (2018) 14410–14417, https://doi.org/10.1021/acsami.8b00952.
[17] R. Jiang, J. Dai, X. Dong, Q. Wang, Z. Meng, J. Guo, Y. Yu, S. Wang, F. Xia, Z. Zhao, X. Lou, B.Z. Tang, Improving image-guided surgical and immunological tumor treatment efficacy by photothermal and photodynamic therapies based on a multifunctional NIR AIEgen, Adv. Mater. 33 (2021), 2101158, https://doi.org/10.1002/adma.202101158.
[18] T. Zhang, J. Zhang, F.-B. Wang, H. Cao, D. Zhu, X. Chen, C. Xu, X. Yang, W. Huang, Z. Wang, J. Wang, Z. He, Z. Zheng, J.W.Y. Lam, B.Z. Tang, Mitochondria-targeting phototheranostics by aggregation-induced NIR-II emission luminogens: modulating intramolecular motion by electron acceptor engineering for multi-modal synergistic therapy, Adv. Funct. Mater. 32 (2022), 2110526, https://doi.org/10.1002/adfm.202110526.
[19] Z. Liu, H. Zou, Z. Zhao, P. Zhang, G.-G. Shan, R.T.K. Kwok, J.W.Y. Lam, L. Zheng, B.Z. Tang, Tuning organelle specificity and photodynamic therapy efficiency by molecular function design, ACS Nano 13 (2019) 11283–11293, https://doi.org/10.1021/acsnano.9b04430.
[20] D. Mao, B. Liu, Biology-oriented design strategies of AIE theranostic probes, Matter 4 (2021) 350–376, https://doi.org/10.1016/j.matt.2020.12.006.
[21] S. Liu, X. Zhou, H. Zhang, H. Ou, J.W.Y. Lam, Y. Liu, L. Shi, D. Ding, B.Z. Tang, Molecular motion in aggregates: manipulating TICT for boosting photothermal theranostics, J. Am. Chem. Soc. 141 (2019) 5359–5368, https://doi.org/10.1021/jacs.8b13889.
[22] S. Gao, G. Wei, S. Zhang, B. Zheng, J. Xu, G. Chen, M. Li, S. Song, W. Fu, Z. Xiao, W. Lu, Albumin tailoring fluorescence and photothermal conversion effect of near-infrared-II fluorophore with aggregation-induced emission characteristics, Nat. Commun. 10 (2019) 2206, https://doi.org/10.1038/s41467-019-10056-9.
[23] Z. Zhao, B.Z. Tang, A divergent and stereoselective synthetic strategy for tetraarylethylene-based AIEgens, Natl. Sci. Rev. 8 (2021), nwab015, https://doi.org/10.1093/nsr/nwab015.
[24] D. Yan, Q. Wu, D. Wang, B.Z. Tang, Innovative synthetic procedures for luminogens showing aggregation-induced emission, Angew. Chem. Int. Ed. 60 (2021) 15724–15742, https://doi.org/10.1002/anie.202006191.
[25] S.L. Yu, H.X. Xiang, J.L. Zhou, T. Qiu, Z.X. Hu, M.F. Zhu, Typical polymer fiber materials: an overview and outlook, Acta Polym. Sin. 51 (2020) 39–54, https://doi.org/10.11777/j.issn1000-3304.2020.19148.
[26] W. Ma, Y. Zhang, S. Pan, Y. Cheng, Z. Shao, H. Xiang, G. Chen, L. Zhu, W. Weng, H. Bai, M. Zhu, Smart fibers for energy conversion and storage, Chem. Soc. Rev. (2021) 7009–7061, https://doi.org/10.1039/D0CS01603A.
[27] T. Huang, J. Zhang, B. Yu, H. Yu, H. Long, H. Wang, Q. Zhang, M. Zhu, Fabric texture design for boosting the performance of a knitted washable textile triboelectric nanogenerator as wearable power, Nano Energy 58 (2019) 375–383, https://doi.org/10.1016/j.nanoen.2019.01.038.
[28] X. Shi, Y. Zuo, P. Zhai, J. Shen, Y. Yang, Z. Gao, M. Liao, J. Wu, J. Wang, X. Xu, Q. Tong, B. Zhang, B. Wang, X. Sun, L. Zhang, Q. Pei, D. Jin, P. Chen, H. Peng, Large-area display textiles integrated with functional systems, Nature 591 (2021) 240–245, https://doi.org/10.1038/s41586-021-03295-8.
[29] M.E. Genovese, E. Colusso, M. Colombo, A. Martucci, A. Athanassiou, D. Fragouli, Acidochromic fibrous polymer composites for rapid gas detection, J. Mater. Chem. 5 (2016) 339–348, https://doi.org/10.1039/C6TA08793K.
[30] Y. Jiang, Y. Cheng, S. Liu, H. Zhang, X. Zheng, M. Chen, M. Khorloo, H. Xiang, B. Z. Tang, M. Zhu, Solid-state intramolecular motions in continuous fibers driven by ambient humidity for fluorescent sensors, Natl. Sci. Rev. 8 (2021), https://doi.org/10.1093/nsr/nwaa135 nwaa135.
[31] Y. Cheng, H. Wang, L. Li, T. Han, X. Liang, L. Dong, Flexible photoluminescent humidity sensing material based on electrospun PVA nanofibers comprising surface-carboxylated QDs, Sensor. Actuator. B Chem. 284 (2019) 258–264, https://doi.org/10.1016/j.snb.2018.12.140.
[32] L. Zhao, Z. Zhang, M. Chen, Y. Liu, T. Wang, X. Li, Fluorescent fibrous mats assembled with self-propagating probes for visual sensing of hydrogen peroxide and choline, Analyst 144 (2019) 5624–5636, https://doi.org/10.1039/C9AN01120J.
[33] L. Zhao, S. Xie, Y. Liu, Q. Liu, X. Song, X. Li, Janus micromotors for motion-capture-lighting of bacteria, Nanoscale 11 (2019) 17831–17840, https://doi.org/10.1039/C9NR05503G.
[34] H. Li, H. Wen, J. Li, J. Huang, D. Wang, B.Z. Tang, Doping AIE photothermal molecule into all-fiber aerogel with self-pumping water function for efficiency solar steam generation, ACS Appl. Mater. Interfaces 12 (2020) 26033–26040, https://doi.org/10.1021/acsami.0c06181.
[35] H. Li, H. Wen, Z. Zhang, N. Song, R.T.K. Kwok, J.W.Y. Lam, L. Wang, D. Wang, B. Z. Tang, Reverse thinking of the aggregation-induced emission principle: amplifying molecular motions to boost photothermal efficiency of nanofibers, Angew. Chem. Int. Ed. 59 (2020) 20371–20375, https://doi.org/10.1002/anie.202008292.
[36] M. Chen, R. Chen, Y. Shi, J. Wang, Y. Cheng, Y. Li, X. Gao, Y. Yan, J.Z. Sun, A. Qin, R.T.K. Kwok, J.W.Y. Lam, B.Z. Tang, Malonitrile-functionalized tetraphenylpyrazine: aggregation-induced emission, ratiometric detection of hydrogen sulfide, and mechanochromism, Adv. Funct. Mater. 28 (2018), 1704689, https://doi.org/10.1002/adfm.201704689.
[37] Y. Jiang, Q. Duan, G. Zheng, L. Yang, J. Zhang, Y. Wang, H. Zhang, J. He, H. Sun, D. Ho, An ultra-sensitive and ratiometric fluorescent probe based on the DTBET process for Hg2+ detection and imaging applications, Analyst 144 (2019) 1353–1360, https://doi.org/10.1039/C8AN02126K.
[38] C. Ma, Z. Li, C. Zhang, G. Xie, Y. Wu, Y. Zhang, J. Mo, X. Liu, K. Wang, D. Xie, Y. Li, Design and synthesis of AIE-based small-molecule and nanofibrous film for fluorescent sensing application, Front. Chem. 9 (2021), 727631, https://doi.org/10.3389/fchem.2021.727631.
[39] K. Li, R.-H. Yu, C.-M. Shi, F.-R. Tao, T.-D. Li, Y.-Z. Cui, Electrospun nanofibrous membrane based on AIE-active compound for detecting picric acid in aqueous solution, Sensor. Actuator. B Chem. 262 (2018) 637–645, https://doi.org/10.1016/j.snb.2018.02.032.
[40] L. Zhao, Z. Zhang, Y. Liu, J. Wei, Q. Liu, P. Ran, X. Li, Fibrous strips decorated with cleavable aggregation-induced emission probes for visual detection of Hg2+, J. Hazard Mater. 385 (2020), 121556 https://doi.org/10.1016/j.jhazmat.2019.121556.
[41] X. Huang, Z. Jiao, Z. Guo, J. Yang, P. Alam, Y. Liu, Y. Men, P. Zhang, H. Feng, S. Yao, B.Z. Tang, Development of reaction-based AIE handy pen for visual detection of toxic vapors, ACS Mater. Lett. 3 (2021) 249–254, https://doi.org/10.1021/acsmaterialslett.0c00516.
[42] M. Gao, G. Xu, R. Zhang, Z. Liu, H. Xia, B. Shao, C. Xue, J. Li, S. Miao, W. Fu, X. Zhang, J. Zhou, X. Jiang, K. Liang, B. Kong, Electrospinning superassembled mesoporous AIEgen–organosilica frameworks featuring diversified forms and superstability for wearable and washable solid-state fluorescence smart sensors, Anal. Chem. 93 (2021) 2367–2376, https://doi.org/10.1021/acs.analchem.0c04226.
[43] G. Tabanelli, Biogenic amines and food quality: emerging challenges and public health concerns, Foods 9 (2020) 859, https://doi.org/10.3390/foods9070859.
[44] D. Doeun, M. Davaatseren, M.-S. Chung, Biogenic amines in foods, Food Sci. Biotechnol. 26 (2017) 1463–1474, https://doi.org/10.1007/s10068-017-0239-3.
[45] V. Feddern, H. Mazzuco, F.N. Fonseca, G.J.M.M.d. Lima, A review on biogenic amines in food and feed: toxicological aspects, impact on health and control measures, Anim. Prod. Sci. 59 (2019) 608–618, https://doi.org/10.1071/AN18076.
[46] A. Yadav, Y. Upadhyay, R.K. Bera, S.K. Sahoo, Vitamin B6 cofactors guided highly selective fluorescent turn-on sensing of histamine using beta-cyclodextrin stabilized ZnO quantum dots, Food Chem. 320 (2020), 126611, https://doi.org/10.1016/j.foodchem.2020.126611.
[47] P. Alam, N.L.C. Leung, J. Zhang, R.T.K. Kwok, J.W.Y. Lam, B.Z. Tang, AIE-based luminescence probes for metal ion detection, Coord. Chem. Rev. 429 (2021), 213693, https://doi.org/10.1016/j.ccr.2020.213693.
[48] D. Wu, L. Chen, W. Lee, G. Ko, J. Yin, J. Yoon, Recent progress in the development of organic dye based near-infrared fluorescence probes for metal ions, Coord. Chem. Rev. 354 (2018) 74–97, https://doi.org/10.1016/j.ccr.2017.06.011.
[49] S. Zhang, J.-M. Yan, A.-J. Qin, J.-Z. Sun, B.-Z. Tang, The specific detection of Cu (II) using an AIE-active alanine ester, Chin. Chem. Lett. 24 (2013) 668–672, https://doi.org/10.1016/j.cclet.2013.05.014.
[50] Y. Liu, I. Cotgreave, L. Atzori, R.C. Grafström, The mechanism of Hg2+ toxicity in cultured human oral fibroblasts: the involvement of cellular thiols, Chem. Biol. Interact. 85 (1992) 69–78, https://doi.org/10.1016/0009-2797(92)90053-N.
[51] K.-H. Kim, E. Kabir, S.A. Jahan, A review on the distribution of Hg in the environment and its human health impacts, J. Hazard Mater. 306 (2016) 376–385, https://doi.org/10.1016/j.jhazmat.2015.11.031.
[52] S. Jiang, S. Chen, Z. Wang, H. Guo, F. Yang, First fluorescence sensor for simultaneously detecting three kinds of IIB elements (Zn2+, Cd2+ and Hg2+) based on aggregation-induced emission, Sensor. Actuator. B Chem. 308 (2020), 127734, https://doi.org/10.1016/j.snb.2020.127734.
[53] E. Schoolaert, R. Hoogenboom, K. De Clerck, Colorimetric nanofibers as optical sensors, Adv. Funct. Mater. 27 (2017), 1702646, https://doi.org/10.1002/adfm.201702646.
[54] Y. Zhang, Y. Li, X. Jia, E.B. Berda, C. Wang, D. Chao, Advanced electrochromic/electrofluorochromic poly(amic acid) toward the colorimetric/fluorometric dual-determination of glycosuria, Mater. Today Chem. 21 (2021), 100497, https://doi.org/10.1016/j.mtchem.2021.100497.
[55] American Diabetes Association, Diagnosis and classification of diabetes mellitus, Diabetes Care 27 (2004) s5–s10, https://doi.org/10.2337/diacare.27.2007.S5.
[56] H.-S. Han, G. Kang, J.S. Kim, B.H. Choi, S.-H. Koo, Regulation of glucose metabolism from a liver-centric perspective, Exp. Mol. Med. 48 (2016) e218, https://doi.org/10.1038/emm.2015.122.
[57] X. Zhang, E. Sucre-Rosales, A. Byram, F.E. Hernandez, G. Chen, Ultrasensitive visual detection of glucose in urine based on the Iodide-promoted etching of gold bipyramids, ACS Appl. Mater. Interfaces 12 (2020) 49502–49509, https://doi.org/10.1021/acsami.0c16369.
[58] R. Cha, D. Wang, Z. He, Y. Ni, Development of cellulose paper testing strips for quick measurement of glucose using chromogen agent, Carbohydr. Polym. 88 (2012) 1414–1419, https://doi.org/10.1016/j.carbpol.2012.02.028.
[59] B. Coşkuner Filiz, Y. Basaran Elalmis, İ.S. Bektaş, A. Kantürk Figen, Fabrication of stable electrospun blended chitosan-poly(vinyl alcohol) nanofibers for designing naked-eye colorimetric glucose biosensor based on GOx/HRP, Int. J. Biol. Macromol. 192 (2021) 999–1012, https://doi.org/10.1016/j.ijbiomac.2021.10.048.
[60] S. Xie, Q. Liu, F. Zhu, M. Chen, L. Wang, Y. Xiong, Y. Zhu, Y. Zheng, X. Chen, AIE-active metal–organic frameworks: facile preparation, tunable light emission, ultrasensitive sensing of copper(II) and visual fluorescence detection of glucose, J. Mater. Chem. C 8 (2020) 10408–10415, https://doi.org/10.1039/D0TC00106F.
[61] Y. Cheng, J. Wang, Z. Qiu, X. Zheng, N.L.C. Leung, J.W.Y. Lam, B.Z. Tang, Multiscale humidity visualization by environmentally sensitive fluorescent

molecular rotors, Adv. Mater. 29 (2017), 1703900, https://doi.org/10.1002/adma.201703900.
[62] K. Ogai, M. Fukuoka, K.-i. Kitamura, K. Uchide, T. Nemoto, Development of a small wireless device for perspiration monitoring, Med. Eng. Phys. 38 (2016) 391–397, https://doi.org/10.1016/j.medengphy.2015.12.009.
[63] Y. Deng, J. Liu, E. Mäder, G. Heinrich, J. Zhang, S. Gao, Water vapor sensing by carbon nanoparticle "skin", Adv. Mater. Interfac. 2 (2015), 1500244 https://doi.org/10.1002/admi.201500244.
[64] L. Zhao, S. Xie, X. Song, J. Wei, Z. Zhang, X. Li, Ratiometric fluorescent response of electrospun fibrous strips for real-time sensing of alkaline phosphatase in serum, Biosens. Bioelectron. 91 (2017) 217–224, https://doi.org/10.1016/j.bios.2016.12.025.
[65] L. Zhao, T. Wang, Q. Wu, Y. Liu, Z. Chen, X. Li, Fluorescent strips of electrospun fibers for ratiometric sensing of serum heparin and urine trypsin, ACS Appl. Mater. Interfaces 9 (2017) 3400–3410, https://doi.org/10.1021/acsami.6b14118.
[66] B.A. Rader, Alkaline phosphatase, an unconventional immune protein, Front. Immunol. 8 (2017), https://doi.org/10.3389/fimmu.2017.00897.
[67] J.-P. Lallès, Intestinal alkaline phosphatase: novel functions and protective effects, Nutr. Rev. 72 (2014) 82–94, https://doi.org/10.1111/nure.12082.
[68] S. Sardiwal, P. Magnusson, D.J.A. Goldsmith, E.J. Lamb, Bone alkaline phosphatase in CKD–mineral bone disorder, Am. J. Kidney Dis. 62 (2013) 810–822, https://doi.org/10.1053/j.ajkd.2013.02.366.
[69] P. Colombatto, A. Randone, G. Civitico, J.M. Gorin, L. Dolci, N. Medaina, F. Oliveri, G. Verme, G. Marchiaro, R. Pagni, P. Karayiannis, H.C. Thomas, G. Hess, F. Bonino, M.R. Brunetto, Hepatitis G virus RNA in the serum of patients with elevated gamma glutamyl transpeptidase and alkaline phosphatase: a specific liver disease, J. Viral Hepat. 3 (1996) 301–306, https://doi.org/10.1111/j.1365-2893.1996.tb00102.x.
[70] Z. Song, R.T.K. Kwok, E. Zhao, Z. He, Y. Hong, J.W.Y. Lam, B. Liu, B.Z. Tang, A ratiometric fluorescent probe based on ESIPT and AIE processes for alkaline phosphatase activity assay and visualization in living cells, ACS Appl. Mater. Interfaces 6 (2014) 17245–17254, https://doi.org/10.1021/am505150d.
[71] L. Zhao, Y. Chen, J. Yuan, M. Chen, H. Zhang, X. Li, Electrospun fibrous mats with conjugated tetraphenylethylene and mannose for sensitive turn-on fluorescent sensing of Escherichia coli, ACS Appl. Mater. Interfaces 7 (2015) 5177–5186, https://doi.org/10.1021/am507593p.
[72] L. Zhao, Y. Liu, Z. Zhang, J. Wei, S. Xie, X. Li, Fibrous testing papers for fluorescence trace sensing and photodynamic destruction of antibiotic-resistant bacteria, J. Mater. Chem. B 8 (2020) 2709–2718, https://doi.org/10.1039/D0TB00002G.
[73] M. Bonnet, E. Buc, P. Sauvanet, C. Darcha, D. Dubois, B. Pereira, P. Déchelotte, R. Bonnet, D. Pezet, A. Darfeuille-Michaud, Colonization of the human gut by E. coli and colorectal cancer risk, Clin. Cancer Res. 20 (2014) 859–867, https://doi.org/10.1158/1078-0432.CCR-13-1343.
[74] Y. Xu, M.M. Hassan, A.S. Sharma, H. Li, Q. Chen, Recent advancement in nano-optical strategies for detection of pathogenic bacteria and their metabolites in food safety, Crit. Rev. Food Sci. Nutr. (2021) 1–19, https://doi.org/10.1080/10408398.2021.1950117.
[75] S.I. El-Kowrany, E.A. El- Zamarany, K.A. El-Nouby, D.A. El-Mehy, E.A. Abo Ali, A. A. Othman, W. Salah, A.A. El-Ebiary, Water pollution in the middle nile delta, Egypt: an environmental study, J. Adv. Res. 7 (2016) 781–794, https://doi.org/10.1016/j.jare.2015.11.005.
[76] H. Shen, J. Wang, H. Liu, Z. Li, F. Jiang, F.-B. Wang, Q. Yuan, Rapid and selective detection of pathogenic bacteria in bloodstream infections with aptamer-based recognition, ACS Appl. Mater. Interfaces 8 (2016) 19371–19378, https://doi.org/10.1021/acsami.6b06671.
[77] O. Lazcka, F.J.D. Campo, F.X. Muñoz, Pathogen detection: a perspective of traditional methods and biosensors, Biosens. Bioelectron. 22 (2007) 1205–1217, https://doi.org/10.1016/j.bios.2006.06.036.
[78] A.B. Pebdeni, M. Hosseini, A. Barkhordari, Smart fluorescence aptasensor using nanofiber functionalized with carbon quantum dot for specific detection of pathogenic bacteria in the wound, Talanta 246 (2022), 123454, https://doi.org/10.1016/j.talanta.2022.123454.
[79] N.A. Patil, P.M. Gore, N. Jaya Prakash, P. Govindaraj, R. Yadav, V. Verma, D. Shanmugarajan, S. Patil, A. Kore, B. Kandasubramanian, Needleless electrospun phytochemicals encapsulated nanofibre based 3-ply biodegradable mask for combating COVID-19 pandemic, Chem. Eng. J. 416 (2021), 129152, https://doi.org/10.1016/j.cej.2021.129152.
[80] I. Ofek, D. Mirelman, N. Sharon, Adherence of Escherichia coli to human mucosal cells mediated by mannose receptors, Nature 265 (1977) 623–625, https://doi.org/10.1038/265623a0.
[81] T. Huang, Y. Zheng, Y. Yan, L. Yang, Y. Yao, J. Zheng, L. Wu, X. Wang, Y. Chen, J. Xing, X. Yan, Probing minority population of antibiotic-resistant bacteria, Biosens. Bioelectron. 80 (2016) 323–330, https://doi.org/10.1016/j.bios.2016.01.054.
[82] Y. Ding, Z. Li, C. Xu, W. Qin, Q. Wu, X. Wang, X. Cheng, L. Li, W. Huang, Fluorogenic probes/inhibitors of β-lactamase and their applications in drug-resistant bacteria, Angew. Chem. Int. Ed. 60 (2021) 24–40, https://doi.org/10.1002/anie.202006635.
[83] L. Li, Z. Li, W. Shi, X. Li, H. Ma, Sensitive and selective near-infrared fluorescent off–on probe and its application to imaging different levels of β-lactamase in staphylococcus aureus, Anal. Chem. 86 (2014) 6115–6120, https://doi.org/10.1021/ac501288e.
[84] M.U. Hadi, M. Khurshid, SARS-CoV-2 detection using optical fiber based sensor method, Sensors 22 (2022) 751, https://doi.org/10.3390/s22030751.
[85] S.-L. Lee, J. Kim, S. Choi, J. Han, G. Seo, Y.W. Lee, Fiber-optic label-free biosensor for SARS-CoV-2 spike protein detection using biofunctionalized long-period fiber grating, Talanta 235 (2021), 122801, https://doi.org/10.1016/j.talanta.2021.122801.
[86] Z. Liu, T. Meng, X. Tang, R. Tian, W. Guan, The promise of aggregation-induced emission luminogens for detecting COVID-19, Front. Immunol. 12 (2021), 635558, https://doi.org/10.3389/fimmu.2021.635558.
[87] R. Chen, C. Ren, M. Liu, X. Ge, M. Qu, X. Zhou, M. Liang, Y. Liu, F. Li, Early detection of SARS-CoV-2 seroconversion in humans with aggregation-induced near-infrared emission nanoparticle-labeled lateral flow immunoassay, ACS Nano 15 (2021) 8996–9004, https://doi.org/10.1021/acsnano.1c01932.
[88] X. Cai, B. Liu, Aggregation-induced emission: recent advances in materials and biomedical applications, Angew. Chem. Int. Ed. 59 (2020) 9868–9886, https://doi.org/10.1002/anie.202000845.
[89] R. Qu, X. Zhen, X. Jiang, Emerging designs of aggregation-induced emission agents for enhanced phototherapy applications, CCS Chem 4 (2022) 401–419, https://doi.org/10.31635/ccschem.021.202101302.
[90] D. Wang, H. Su, R.T.K. Kwok, X. Hu, H. Zou, Q. Luo, M.M.S. Lee, W. Xu, J.W. Y. Lam, B.Z. Tang, Rational design of a water-soluble NIR AIEgen, and its application in ultrafast wash-free cellular imaging and photodynamic cancer cell ablation, Chem. Sci. 9 (2018) 3685–3693, https://doi.org/10.1039/C7SC04963C.
[91] M.M.S. Lee, W. Xu, L. Zheng, B. Yu, A.C.S. Leung, R.T.K. Kwok, J.W.Y. Lam, F.-J. Xu, D. Wang, B.Z. Tang, Ultrafast discrimination of Gram-positive bacteria and highly efficient photodynamic antibacterial therapy using near-infrared photosensitizer with aggregation-induced emission characteristics, Biomaterials 230 (2020), https://doi.org/10.1016/j.biomaterials.2019.119582, 119582.
[92] F. Hu, S. Xu, B. Liu, Photosensitizers with aggregation-induced emission: materials and biomedical applications, Adv. Mater. 30 (2018), 1801350, https://doi.org/10.1002/adma.201801350.
[93] Z. Zhao, C. Chen, W. Wu, F. Wang, L. Du, X. Zhang, Y. Xiong, X. He, Y. Cai, R.T. K. Kwok, J.W.Y. Lam, X. Gao, P. Sun, D.L. Phillips, D. Ding, B.Z. Tang, Highly efficient photothermal nanoagent achieved by harvesting energy via excited-state intramolecular motion within nanoparticles, Nat. Commun. 10 (2019) 768, https://doi.org/10.1038/s41467-019-08722-z.
[94] N. Alifu, A. Zebibula, J. Qi, H. Zhang, C. Sun, X. Yu, D. Xue, J.W.Y. Lam, G. Li, J. Qian, B.Z. Tang, Single-molecular near-infrared-II theranostic systems: ultrastable aggregation-induced emission nanoparticles for long-term tracing and efficient photothermal therapy, ACS Nano 12 (2018) 11282–11293, https://doi.org/10.1021/acsnano.8b05937.
[95] R. Dong, Y. Li, M. Chen, P. Xiao, Y. Wu, K. Zhou, Z. Zhao, B.Z. Tang, In situ electrospinning of aggregation-induced emission nanofibrous dressing for wound healing, Small Methods (2022), 2101247, https://doi.org/10.1002/smtd.202101247.
[96] B. Li, D. Wang, M.M.S. Lee, W. Wang, Q. Tan, Z. Zhao, B.Z. Tang, X. Huang, Fabrics attached with highly efficient aggregation-induced emission photosensitizer: toward self-antiviral personal protective equipment, ACS Nano 15 (2021) 13857–13870, https://doi.org/10.1021/acsnano.1c06071.
[97] Z. Zhang, M. Kang, H. Tan, N. Song, M. Li, P. Xiao, D. Yan, L. Zhang, D. Wang, B. Z. Tang, The fast-growing field of photo-driven theranostics based on aggregation-induced emission, Chem. Soc. Rev. 51 (2022) 1983–2030, https://doi.org/10.1039/D1CS01138C.
[98] M. Kang, C. Zhou, S. Wu, B. Yu, Z. Zhang, N. Song, M.M.S. Lee, W. Xu, F.-J. Xu, D. Wang, L. Wang, B.Z. Tang, Evaluation of structure–function relationships of aggregation-induced emission luminogens for simultaneous dual applications of specific discrimination and efficient photodynamic killing of Gram-positive bacteria, J. Am. Chem. Soc. 141 (2019) 16781–16789, https://doi.org/10.1021/jacs.9b07162.
[99] World Health Organization, COVID-19 Weekly Epidemiological Update, Edition 89, 27 April 2022, World Heal. Organ, 2022. https://apps.who.int/iris/handle/10665/353609.
[100] J. Zhou, Z. Hu, F. Zabihi, Z. Chen, M. Zhu, Progress and perspective of antiviral protective material, Adv. Fiber Mater. 2 (2020) 123–139, https://doi.org/10.1007/s42765-020-00047-7.
[101] A.A. Chughtai, H. Seale, C.R. Macintyre, Effectiveness of cloth masks for protection against severe acute respiratory syndrome coronavirus 2, Emerg. Infect. Dis. 26 (2020) 1–5, https://doi.org/10.3201/eid2610.200948.
[102] S. Sharma, R. Pinto, A. Saha, S. Chaudhuri, S. Basu, On secondary atomization and blockage of surrogate cough droplets in single- and multilayer face masks, Sci. Adv. 7 (2021), eabf0452, https://doi.org/10.1126/sciadv.abf0452.
[103] S. Sangkham, Face mask and medical waste disposal during the novel COVID-19 pandemic in Asia, Case Study Chem. Env. Eng. 2 (2020), 100052, https://doi.org/10.1016/j.cscee.2020.100052.
[104] M. Li, H. Wen, H. Li, Z.-C. Yan, Y. Li, L. Wang, D. Wang, B.Z. Tang, AIEgen-loaded nanofibrous membrane as photodynamic/photothermal antimicrobial surface for sunlight-triggered bioprotection, Biomaterials 276 (2021) 121007, https://doi.org/10.1016/j.biomaterials.2021.121007.
[105] H. Li, W. Zhu, M. Li, Y. Li, R.T.K. Kwok, J.W.Y. Lam, L. Wang, D. Wang, B.Z. Tang, Side area-assisted 3D evaporator with antibiofouling function for ultra-efficient solar steam generation, Adv. Mater. 33 (2021), 2102258, https://doi.org/10.1002/adma.202102258.
[106] S. Liu, G. Feng, B.Z. Tang, B. Liu, Recent advances of AIE light-up probes for photodynamic therapy, Chem. Sci. 12 (2021) 6488–6506, https://doi.org/10.1039/D1SC00045D.
[107] X. Gu, X. Zhang, H. Ma, S. Jia, P. Zhang, Y. Zhao, Q. Liu, J. Wang, X. Zheng, J.W. Y. Lam, D. Ding, B.Z. Tang, Corannulene-incorporated AIE nanodots with highly

suppressed nonradiative decay for boosted cancer phototheranostics in vivo, Adv. Mater. 30 (2018), 1801065, https://doi.org/10.1002/adma.201801065.
[108] D. Wang, M.M.S. Lee, W. Xu, G. Shan, X. Zheng, R.T.K. Kwok, J.W.Y. Lam, X. Hu, B.Z. Tang, Boosting non-radiative decay to do useful work: development of a multi-modality theranostic system from an AIEgen, Angew. Chem. Int. Ed. 58 (2019) 5628–5632, https://doi.org/10.1002/anie.201900366.
[109] S. Liu, Y. Li, H. Zhang, Z. Zhao, X. Lu, J.W.Y. Lam, B.Z. Tang, Molecular motion in the solid state, ACS Mater. Lett. 1 (2019) 425–431, https://doi.org/10.1021/acsmaterialslett.9b00292.